

# **Image processing algorithms for compensation of spatially variant blur**

Masters thesis  
Tekniska Högskolan i Linköping  
by

**Mathias Andersson**

Reg nr: LiTH-ISY-EX-05/3633-SE  
Linköping 2005



# **Image processing algorithms for compensation of spatially variant blur**

Masters thesis  
Tekniska Högskolan i Linköping  
by

**Mathias Andersson**


Reg nr: LiTH-ISY-EX-05/3633-SE

Supervisor: **Amritpal Singh**

Examiner: **Klas Nordberg**

Linköping 2005-05-10.



	<b>Avdelning, Institution</b> Division, Department  Institutionen för systemteknik 581 83 LINKÖPING	<b>Datum</b> Date 2005-05-10						
<b>Språk</b> Language Svenska/Swedish X Engelska/English	<b>Rapporttyp</b> Report category Licentiatavhandling X Examensarbete C-uppsats D-uppsats Övrig rapport _____	<table border="1"> <tr> <td colspan="2"><b>ISBN</b></td> </tr> <tr> <td colspan="2"><b>ISRN</b> LITH-ISK-EX--05/3633--SE</td> </tr> <tr> <td><b>Serietitel och serienummer</b> Title of series, numbering</td> <td><b>ISSN</b> _____</td> </tr> </table>	<b>ISBN</b>		<b>ISRN</b> LITH-ISK-EX--05/3633--SE		<b>Serietitel och serienummer</b> Title of series, numbering	<b>ISSN</b> _____
<b>ISBN</b>								
<b>ISRN</b> LITH-ISK-EX--05/3633--SE								
<b>Serietitel och serienummer</b> Title of series, numbering	<b>ISSN</b> _____							
<b>URL för elektronisk version</b> <a href="http://www.ep.liu.se/exjobb/isy/2005/3633/">http://www.ep.liu.se/exjobb/isy/2005/3633/</a>								
<table border="1"> <tr> <td><b>Titel</b> Title</td> <td>Image processing algorithms for compensation of spatially variant blur.</td> </tr> <tr> <td><b>Författare</b> Author</td> <td>Mathias Andersson</td> </tr> </table>			<b>Titel</b> Title	Image processing algorithms for compensation of spatially variant blur.	<b>Författare</b> Author	Mathias Andersson		
<b>Titel</b> Title	Image processing algorithms for compensation of spatially variant blur.							
<b>Författare</b> Author	Mathias Andersson							
<b>Sammanfattning</b> Abstract This report addresses the problem of software correction of spatially variant blur in digital images. The problem arises when the camera optics contains flaws, when the scene contains multiple moving objects with different relative motion or the camera itself is i.e. rotated. Compensation through deconvolving is impossible due to the shift-variance in the PSF hence alternative methods are required. There are a number of suggested methods published. This report evaluates two methods.								
<b>Nyckelord</b> Keyword spatially variant, blur, shift-variant, image restoration								



# Abstract

This report addresses the problem of software correction of spatially variant blur in digital images. The problem arises when the camera optics contains flaws, when the scene contains multiple moving objects with different relative motion or the camera itself is i.e. rotated. Compensation through deconvolution is impossible due to the shift-variance in the PSF hence alternative methods are required. There are a number of suggested methods published. This report evaluates two methods.

**Keywords:** spatially variant, blur, shift-variant





# Notation

This section introduces the notation and symbols used in this report.

## Symbols

$\boldsymbol{x}, \boldsymbol{X}$	Boldface letters are used for vectors, matrices and sets.
$\boldsymbol{s}, \boldsymbol{t}$	Coordinates in $\mathbb{R}^2$ .
$\boldsymbol{\omega}$	Coordinates in the 2D Fourier domain.
$P(\boldsymbol{\omega})$	The function $p(\boldsymbol{s})$ in the 2D Fourier domain.

## Operators and functions

$\mathcal{F}(g)$	Fourier transform of function $g(\boldsymbol{t})$ .
$P^*$	Complex conjugate of $P$
$\boldsymbol{P}^T$	Transpose of $\boldsymbol{P}$

## Acronyms

SNR	Signal-to-Noise Ratio is a measure of image fidelity defined by equation (4.1).
ME	Mean Error is a measure of image fidelity defined by equation (4.4).
PSF	Point Spread Function describes the blurring operator.



# Contents

<b>1</b>	<b>Introduction</b>	<b>1</b>
1.1	Document structure . . . . .	3
<b>2</b>	<b>Problem description</b>	<b>5</b>
2.1	Blurring . . . . .	5
2.2	Imaging model and restoration . . . . .	7
2.3	Noise . . . . .	9
2.4	Optical aberrations . . . . .	10
2.5	Goal of this report . . . . .	10
2.6	Difficulties . . . . .	11
<b>3</b>	<b>Methods</b>	<b>13</b>
3.1	Choice of methods . . . . .	13
3.2	Landweber method . . . . .	13
3.3	Interpolation method . . . . .	14
3.4	Performance . . . . .	17
3.4.1	Landweber method . . . . .	17
3.4.2	Interpolation method . . . . .	18
3.5	Limitations . . . . .	18
<b>4</b>	<b>Evaluation</b>	<b>21</b>
4.1	Test images . . . . .	21
4.2	Generation of synthetic blurs . . . . .	22
4.3	Evaluation methods . . . . .	24
<b>5</b>	<b>Results</b>	<b>27</b>
5.1	Visual Comparison . . . . .	27
5.1.1	Shift-invariant PSF . . . . .	28
5.1.2	Shift-variant PSF . . . . .	31
5.2	Varying blur size . . . . .	38
5.3	Varying noise . . . . .	41
5.4	Varying PSF estimate . . . . .	44
5.5	Varying number of PSF estimates . . . . .	47
5.6	Coma . . . . .	50

<b>6</b>	<b>Discussion</b>	<b>53</b>
6.1	Summary of results . . . . .	53
6.2	Further research . . . . .	54
6.3	Fulfillment of goals . . . . .	54
<b>A</b>	<b>Fast matrix-vector multiplication</b>	<b>57</b>
A.1	Circulant matrices . . . . .	57
A.2	Toeplitz matrices . . . . .	57

# Chapter 1

## Introduction

Imaging, capturing images with some kind of sensor, is an important tool in many areas. The images captured are used in a number of applications which all have their own demands on the quality of the captured image. In the most basic case, detection, it might be enough to be able to tell whether there is something in the area captured or not. In other cases it might be necessary to be able to tell what type of object has been captured i.e. a car, a house etc. In more advanced applications identification of the object, or even parts of an object such as a vehicles registration number, may be required.

Naturally the completion of the different tasks (detection, classification, identification) is dependent on the quality of the captured image, the more information is to be extracted the better quality is required.

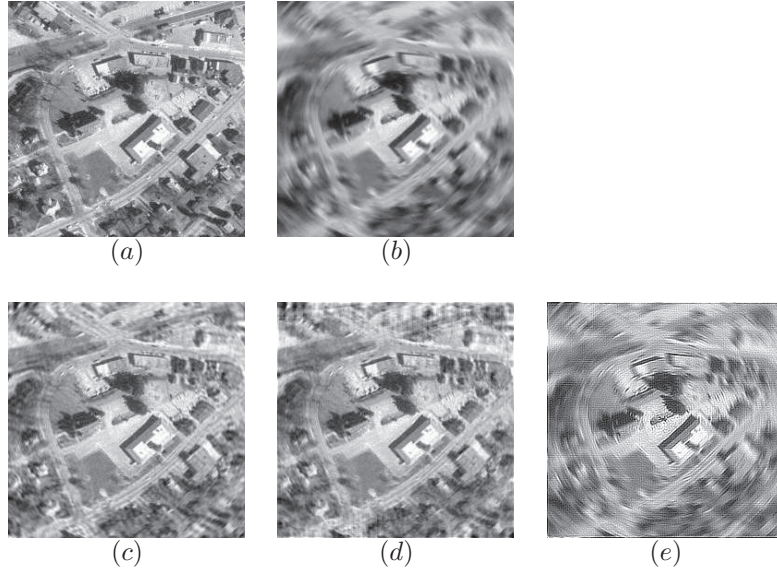
The quality of the captured image is in some cases degraded in various ways which creates the demand for image restoration, restoration of image quality.

Image restoration is an important tool in extracting information from images. A reoccurring problem in image processing is blur. Blurring occurs in a variety of situations i.e. imperfections in optical systems, atmospheric interference, movement of camera/object when using a sensor.

Some sensors need very long exposure times (up to 30 ms) which means that even very small motions can lead to severe blurring. New cheaper IR-sensors, such as micro bolometers [1], are emerging and they have these kind of long exposure times which makes them more noise resistant but as a trade-off are more prone to produce blurry images.

There are two groups of blur, shift-variant and shift-invariant. The main difference between the two lies in how the blur affects different parts of the image. The latter affects the whole image in the same way whereas the former affects different parts of the image in different ways. Figure 1.1 shows an example of an image blurred by shift-variant rotation blur and the results after restoration with three different methods.

A practical example; A missile with a camera mounted on it is targeting a moving vehicle on the ground as it moves towards it, rolling as it turns. In this



**Figure 1.1.** (a) Original image. (b) Image blurred by shift-variant (rotation) blur. (c) and (d) Image restored with the two methods examined in this report. (e) Restored with wiener filter.

basic example we encounter three different blurs that arise from motion only. The moving vehicle will be blurred along its path, the whole image will be blurred since the missile is traveling at great speed and even turning! This is not all. Blur can also be caused by aberrations in the missiles' optics and by atmospheric effects.

Another example; A static camera monitors a section of road where cars pass at high speed. When it is dark outside, the camera must use long exposure times which leads to the cars appearing blurry in the image due to their movement. Since the background varies slowly or not at all the only part of the image blurred is the car, hence shift-variant blur. Again the optics and atmosphere can make the blurring more severe.

If the camera instead had been mounted inside the car, looking out a side window, the whole view would be blurred. In this example though, the whole image would be blurred the same way, by the same sideways motion. The blur is shift-invariant.

Both types can to some extent be corrected mechanically [11] although the implementation often becomes expensive and has practical limitations. In the case of rotation blur for example, the camera, or rather the optics, can be mounted in a way so that it stays aligned with the scene rather than rotates with the body it is mounted in.

Hardware solutions are preferred in critical applications but in cost sensitive applications they are too expensive both during development and during production.

If restoration could be performed in software it would be cheaper and probably more space-efficient. In some cases, where image processing is already in use, it would probably just be a matter of upgrading the software to gain better performance. With the fast development in computer performance more advanced restoration methods can be used.

The restoration of shift-invariant blur is not as complicated as its shift-variant counter-part but it is still very complicated. Mostly because it is an ill-posed problem which among other things leads to a small error in the input image generating a severe error in the restored image. The shift-invariant problem can be solved with direct inverse methods such as the wiener filter. In some cases of shift-variant, for instance rotational blur, the direct inverse methods can be used by performing a transformation of the image to plane-polar coordinates. In plane-polar coordinates both rotation and zoom blur can be seen as shift-invariant, thus the direct inverse methods can be used. However, if there is a mix of two blurs the transformation method may not work since the transformed image may result a shift-variant PSF.

The methods presented in this report aims to restore images blurred by shift-variant blur. The shift-variance of the PSF adds several difficulties to the problem and the need to solve the problem of restoration in its general form adds several more. The shift-invariant case is a reduced case of the general problem which is much easier to solve. Thus, the methods presented should also be able to solve the shift-invariant problem.

## 1.1 Document structure

First a more in-depth description of the problem as well as a model describing it will be presented in chapter 2. After this the restoration methods are introduced and discussed briefly in chapter 3. Chapter 4 defines the test setup by describing what images were used, how they were blurred and finally the measures used during testing. The results of the testing is presented in chapter 5. Chapter 6 discusses the implications of the test results as well as ideas and thoughts surrounding the methods and their use.





## Chapter 2

# Problem description

This chapter begins with describing blurring in more detail and introduces a model of the image formed in an image capturing system. Furthermore, optical aberrations and noise are discussed.

### 2.1 Blurring

When an image is captured in a digital imaging system it is projected from the object-space to the image-plane. In the ideal case one point in the object-plane projects to one point in the image-plane but this is often not the case. Instead one point in the object plane spreads out over several points in the image plane. This is because each point of in object scene is blurred by a number of phenomena, before finally being projected onto the image plane. How the point is spread over the image plane is described by the PSF, point spread function [16]. Figure 2.1(a) illustrates a basic PSF, points are spread out according to a Gaussian function.

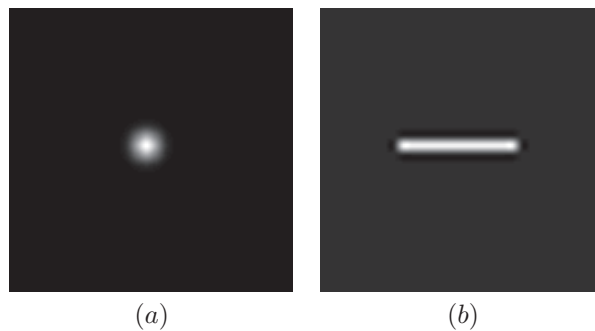


**Figure 2.1.** Two examples of PSFs. (a) is a Gaussian PSF which results in general “out-of-focus blur” and (b) corresponds to horizontal sweeping motion.

Figure 2.2 shows a simple schematic of an imaging system, showing the way

the light travels from object-space to image-plane. This is discussed in more detail in section 2.2. Below follows a brief summary of different causes of blurring in a typical imaging system.

First are the atmospheric effects i.e. temperature differences or turbulence in the air. Temperature differences leads to the light passing through volumes of air with different refractive index thus deviating it from its path. However, such effects are not considered in this report.

After traveling through the air there is the optical system of the camera. First there is diffraction which occurs when the light passes through the aperture of the imaging system, this might lead to a certain amount of blurring. Further blurring can be the result if the optical system is out of focus. The lens system might contain other imperfections and properties that can cause aberrations which can severely deform the resulting image in several ways [2]. Some of the most common aberrations are described in section 2.4.

If the camera is not held still during exposure a given point in the object-scene is “sweep-ed” over several points in the image plane resulting in blurring of the point. A similar effect arises when an object in the scene being captured is moving, then the points of that particular object are blurred. Figure 2.1(b) illustrates a PSF corresponding to a linear sweeping horizontal motion.

Apart from blurring the image may also be affected by various types of noise. Some effects and causes of noise are discussed in section 2.3.

If the image is to be presented to a human observer there are a few more sources of blur. First there may be image processing algorithm applied to the image. They may improve or degrade the image depending on their purpose. This is by the way where restoration algorithms, such as the ones examined in this report, are applied.

After image processing the images are presented on a screen which may suffer from defects that causes blur. Finally the image reaches the human eye which also contains optical flaws that causes blur. These flaws are however to some extent compensated for by the nervous system.

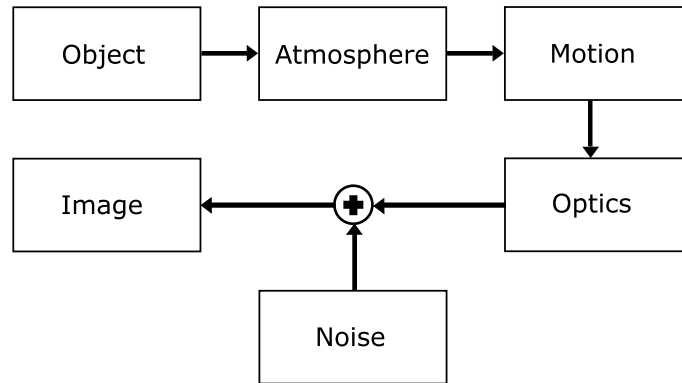


**Figure 2.2.** Schematics of a simple imaging system with different sources of blur.

## 2.2 Imaging model and restoration

To handle the problem of restoring images that have been blurred by the processes described above a mathematical model is needed. The model used in this report is presented below.

The PSF affects the capturing of the object scene,  $o(\mathbf{s})$ , producing an image,  $i(\mathbf{t})$ , which is a modified version of the scene.  $i$  and  $o$  describes the intensities of the image and the object scene;  $\mathbf{s}, \mathbf{t} \in \mathbb{R}^2$ . The capturing of an image given a PSF and in presence of noise can be expressed as

$$i(\mathbf{t}) = \int_{\mathbf{s}} p(\mathbf{s}, \mathbf{t}) o(\mathbf{s}) d\mathbf{s} + n(\mathbf{t}). \quad (2.1)$$

The only case where  $i(\mathbf{t})$  is identical to the scene is when there is no noise and

$$p(\mathbf{s}, \mathbf{t}) = \delta(\mathbf{s} - \mathbf{t}), \quad (2.2)$$

where  $\delta$  is the Dirac function.

As seen in figure 2.2 the image can be affected by several PSFs, one for each kind of blur that can arise in the steps in the image capturing process, and by noise. The effects of all PSFs acting together can be calculated and represented by a single PSF by step-wise using the equation for image capture above. Studying the optical effects and assuming the noise is only present in the detector due to the detector electronics, the cumulative PSF,  $p_c$ , at each step in the blurring process described in figure 2.2, where  $n$  denotes the step and one additional PSF is one step, is calculated as

$$p_c^{(n+1)}(\mathbf{t}) = \int_{\mathbf{s}} p_n(\mathbf{s}, \mathbf{t}) p_c^{(n)}(\mathbf{s}) d\mathbf{s}. \quad (2.3)$$

Equation 2.1 is the general integral equation to be solved in image restoration. In the case of shift-variant a PSF the integral equation 2.1 have to be solved. This equation is also known as the Fredholm equation.

In the case of shift-invariant PSFs, which is one common assumption in image restoration algorithms, the following applies

$$p(\mathbf{s}, \mathbf{t}) = p(\mathbf{s} - \mathbf{t}), \quad (2.4)$$

and equation 2.1 reduces to the convolution integral 2.5 and the restoration is called *deconvolution*.

$$i(\mathbf{t}) = \int_{\mathbf{s}} p(\mathbf{s} - \mathbf{t}) o(\mathbf{s}) d\mathbf{s} + n(\mathbf{t}). \quad (2.5)$$

In the Fourier domain the convolution integral can be written as

$$\mathcal{F}(i) = \mathcal{F}(p)\mathcal{F}(o) + \mathcal{F}(n), \quad (2.6)$$

or without the presence of noise as

$$\mathcal{F}(i) = \mathcal{F}(p)\mathcal{F}(o). \quad (2.7)$$

The restoration in the frequency domain can now be obtained by multiplying both sides with the inverse of  $\mathcal{F}(p)$ ,

$$(\mathcal{F}(p))^{-1}\mathcal{F}(i) = \mathcal{F}(o). \quad (2.8)$$

Methods like this, where you arrive at the restored image in only one iteration using an approximative inverse to the PSF, are also called direct inversion method.

There are problems though. The blurring functions acts as a low-pass filter which means it suppresses high frequencies, often to values near zero. This is a problem if the image is noisy because during restoration high-frequency contents, where noise often dominates over the signal, will be amplified almost indefinitely. To avoid this modified direct inverse filters like the Wiener filter can be used [5].

One variant of the Wiener filter suppresses noise by using information about the spectra of the image and the noise. Combined with the effort to get an inverse filter one possible deconvolution filter is

$$O(\omega) = \frac{P^*(\omega)\phi_I}{|P(\omega)|^2\phi_I + \phi_n}. \quad (2.9)$$

Direct inverse methods will however produce poor results when applied to images degraded by shift-variant blur since they don't take into account the spatial variance of the PSF, often the restored image is severely distorted rendering the inversion meaningless. This is not limited to direct inverse methods but also applies to all restoration methods that doesn't deal with the shift-variance of the PSF. Furthermore, a side-effect of noise suppression is that finer details of the image will be lost.

This report deals with the shift-variant case and two methods are examined. Both methods examined in this report solve the integral equation (2.1) iteratively. There are a large number of iterative methods for this and the examined restoration methods each use a different one. They are the Conjugate Gradient[13] method and the Landweber method [9] and they both yield a least-squares solution to the problem. Direct inverse methods can be used to restore shift-variant blur in special cases by transforming the image to domain where the blur is shift-invariant [8].

For these methods to be useful the problem must be expressed in discrete form which is natural since they are to be applied to digital images.

In discrete form equation (2.1) can be expressed as

$$i(\mathbf{t}) = \sum_{\mathbf{s} \in \mathbb{R}^2} p(\mathbf{s}, \mathbf{t})o(\mathbf{s}) + n(\mathbf{t}), \quad (2.10)$$

which in turn can be written on matrix-form as

$$\mathbf{i} = \mathbf{H}\mathbf{o} + \mathbf{n}, \quad (2.11)$$

where  $\mathbf{H} \in \mathbb{R}^{n \times n}$  and  $n$  is the number of pixels in the sampled versions of the images  $i(t)$  and  $o(s)$ .  $\mathbf{i}$  and  $\mathbf{o}$  are vectors formed by taking the columns of  $i(t)$  and

$o(s)$  respectively and stacking them on top of each other as shown below

$$\begin{pmatrix} i_{1,1} \\ \vdots \\ i_{1,n} \\ i_{2,1} \\ \vdots \\ i_{n,n} \end{pmatrix} = \begin{pmatrix} h_{1,1} & \cdot & \cdot & \cdot & \cdot & h_{m,1} \\ \cdot & \cdot & & & & \cdot \\ \cdot & & \cdot & & & \cdot \\ \cdot & & & \cdot & & \cdot \\ \cdot & & & & \cdot & \cdot \\ h_{1,m} & \cdot & \cdot & \cdot & \cdot & h_{m,m} \end{pmatrix} \begin{pmatrix} o_{1,1} \\ \cdot \\ o_{1,n} \\ o_{2,1} \\ \cdot \\ o_{n,n} \end{pmatrix}. \quad (2.12)$$

Each row in  $\mathbf{H}$  represents the local PSF for one pixel in the output image.  $\mathbf{H}$  is simply a digital filter [6]. For a shift-invariant PSF this results in a Toeplitz matrix, see appendix A. Both restoration methods in this report assumes the PSF to be locally shift in-variant to some extent, see chapter 3 thus the special structure of Toeplitz matrices can be exploited.

Both  $\mathbf{i}$  and  $\mathbf{o}$  are assumed to have the same dimensions. This is true throughout this report but in the general case they may very well differ. Also, the methods evaluated does not deal with the noise explicitly but limits the effects of the noise by stopping iterations early. This leads to further simplification of the problem to

$$\mathbf{i} = \mathbf{H}\mathbf{o}. \quad (2.13)$$

## 2.3 Noise

The registration of the light from the scene is carried out by integrating the light hitting a number of electronic detector elements. These elements and the electronics in the rest of the imaging system suffer from imperfections that introduces noise. Another source of noise is the individual photons that hit the detector elements, called photon noise.

Another kind of noise arises from the construction of the sensor and is called *pattern noise*. The sensor array is built from a large number of sensors, all with slightly different properties which leads to a degraded output image. This kind of noise is often highly correlated in time and sometimes also spatially. This makes it quite different from what is commonly regarded as noise. Pattern noise can be corrected to some extent by calibrating the sensor although with IR-sensors calibration is difficult.

Although the model described above does not incorporate noise it is still present in the images that are to be restored. The problem of image restoration is far more complicated when noise is involved. Even if a well defined inverse to  $\mathbf{H}$  exists the noise makes it impossible to achieve a “perfect” restoration.

The noise in sensors is often modeled as white and additive and is induced by the sensor and the electronics around it. Knowing this much about the noise allows for slightly better compensation when using methods that can take the characteristics of the noise in account.

When studying integrating sensors photon noise is also a problem because the sensor “counts” individual photons. This type of noise depends on the intensity of

the scene that is being captured. By increasing the integration time of the sensor this problem can be diminished but as a downside the sensor will be more sensitive to motion blur.

## 2.4 Optical aberrations

As mentioned above optical aberrations are often present in imaging systems and are therefore interesting to study. There are ways to design optical systems that are almost free from aberrations but they are both difficult to design and expensive. A short description of the most common aberrations follows.

Spherical aberration, which comes from the spherical shape of the lenses, blurs the point because light that passes through the lens at different distances from the optical axis have different focal depths.

Astigmatism which makes the point form an oblong shape perpendicular to the optical axis instead of a more dot-like one. The effect is stronger towards the edges.

Coma, which is one of the most difficult aberrations to correct, which comes from the lenses' inability to focus several rays from the same object point into the same point on the sensor because of the difference in inclination angle against the lens. Figure 2.3 illustrates a coma PSF.

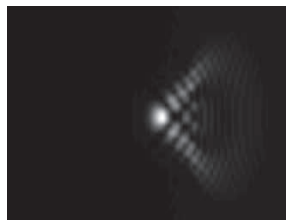


**Figure 2.3.** Coma PSF

When capturing images containing a broad spectra of wavelengths chromatic aberration is also a problem, the non-monochromatic light is separated into it's different wavelengths when passing through the lenses.

## 2.5 Goal of this report

The goal of this report is to search in literature for methods that can solve the problem of compensating for shift-variant blurs in digital images, implement them and finally evaluate them. The evaluation process should include aspects such as noise tolerance, sensitivity to errors in the PSF estimate, capability to compensate for different amount of blur. The evaluation should reveal if the methods are useful and also how and if it is possible to further improve them.

## 2.6 Difficulties

With the model at hand and the various problems such as noise and blur in mind a number of difficulties can be expected during implementation of the evaluated methods.

When solving equation 2.13 in practice  $\mathbf{H}$  is seldom at hand. In best case all or some rows of  $\mathbf{H}$  are known but normally  $\mathbf{H}$  is largely unknown. Methods dealing with the worst case, where  $\mathbf{H}$  is totally unknown, are called *blind deconvolution* methods and are generally complicated and produce varying results. The problem is that such methods must estimate the PSF from features found in the image.

Even when  $\mathbf{H}$  is partly known the problem described by equation 2.13 is ill-posed because  $\mathbf{H}$  lacks a well defined inverse.

The methods examined in this report have two different approaches to dealing with the problem of defining the unknown parts of  $\mathbf{H}$ .

Dealing with  $\mathbf{H}$  explicitly is resource demanding since it will be  $(65535 \times 65535)$  for an image of size  $(256 \times 256)$ . Therefore some way of dealing with  $\mathbf{H}$  implicitly or piece-wise would be preferable.

There are other problems, not directly related to the state of  $\mathbf{H}$ , that will arise. During restoration edge-effects, such as introduction of various artifacts and ringing, will occur. This because all information needed to restore the image is not available. When processing the areas near the edges the filters will partially cover areas outside of the image much in the same way as when the PSF was applied to begin with, see 4.2. The problem is that during reconstruction the information outside the image must be substituted. What to substitute these areas with to minimize errors is one problem to deal with.

Another difficult problem is the noise. Since the model doesn't incorporate noise the methods may very well break down during restoration due to noise.

As mentioned in section 4.3 measuring the quality of the restored image will be a problem. Several methods are used in this report but they all suffer from drawbacks.





## Chapter 3

# Methods

This chapter gives a brief description of the two methods studied and the limitations that exists in the implementations in this report.

### 3.1 Choice of methods

The two methods presented in this report were chosen as suitable candidates for the solution to the problem presented in chapter 2. The search for suitable methods was mainly conducted in scientific articles and reports covering the subject of image restoration. Most articles deals with spatially invariant PSFs and were therefore discarded on that ground. Among the assembled reports and articles, the ones that dealt with shift-variant blur were more closely inspected to see if their intended areas of application matched the needs in this report. Since knowledge of the PSF could be assumed, methods that covered the area of blind restoration were discarded. The two methods finally chosen were the “Landweber method” and the “Interpolation method”, both solving the problem in different ways.

### 3.2 Landweber method

This method is based on an article[15] by H.J. Trussel et. al.

The basis of this method is the assumption that the blur varies slowly over the image, hence can be regarded as locally shift-invariant. The image is then segmented into a number of areas in which the PSF is regarded as shift-invariant and the local instance of equation 2.13 is solved with the Landweber iterations.

The captured image  $\mathbf{i}$  is formed as follows

$$\mathbf{i} = \mathbf{H}\mathbf{o}. \quad (3.1)$$

$\mathbf{H}$  is the convolution matrix that describes the PSF in each point of the image and  $\mathbf{o}$  is the scene being captured.  $\mathbf{i}$  and  $\mathbf{o}$  are  $N \times 1$  and  $\mathbf{H}$  is  $N \times N$ .

To solve this problem efficiently when the PSF is space-variant the image is split into segments where the local PSF can be treated as space-invariant. For this to be an accurate assumption the PSF must not vary too quickly spatially. Making this assumption is helpful since a space-invariant PSF corresponds to a Toeplitz formed convolution matrix and for such there are methods for fast matrix-vector multiplication using circulant approximations of the Toeplitz matrix, see Appendix A.

The Landweber iteration produces a least squares solution to the system in 3.1 using the equation below

$$\mathbf{o}_n^{k+1} = \mathbf{o}_n^k + \beta \mathbf{H}_n^T (\mathbf{i}_n - \mathbf{H}_n \mathbf{o}_n^k). \quad (3.2)$$

$n$  denotes the processed segment and  $k$  denotes the iteration. Each segment consists of a center-part, where the PSF is assumed to be invariant, and an overlapping part, which overlaps into neighboring segments. This overlap is important to avoid local edge-effects.

Each segment is iterated over until

$$|\mathbf{i}_{nc} - \mathbf{H}_{nc} \mathbf{o}_{nc}| < \epsilon, \quad (3.3)$$

or

$$k = \text{maxit}, \quad (3.4)$$

where  $\epsilon$  is the error tolerance and *maxit* is the maximum number of iterations allowed.  $c$  denotes the center, non-overlapping, part of the segment.

Since each segment is dependent on neighboring segments during iteration due to the overlap the convergence of each segment is also dependent on their neighbors. Thus when all segments are processed the method restarts, iterating over all segments once more. Since the segmentation of the image leads to a certain blockiness the process is restarted with a random offset. This ensures that the borders of the segments during the second iteration won't align and amplify any border-effect. The number of offset restarts is denoted *shakes*.

To further increase performance the landweber iterations were modified to be adaptive[10] by optimizing  $\beta$  in each step.

The Landweber method is the more computationally expensive, see section 3.4, of the two methods. This is not necessarily a problem as long as it is used for offline restoration. Implementing it for use in real-time systems may be possible if it is implemented in dedicated hardware such as programmable logic.

Concerning image quality the Landweber method produces images with quality similar to the interpolation method although a bit more blur remaining.

The Landweber method suffers from instabilities. This has become apparent during testing when Gaussian blur caused the method to diverge.

### 3.3 Interpolation method

The basis of the interpolation method is the assumption that the blur varies slowly and can be seen as piecewise linear. The PSF is known in a number of points and

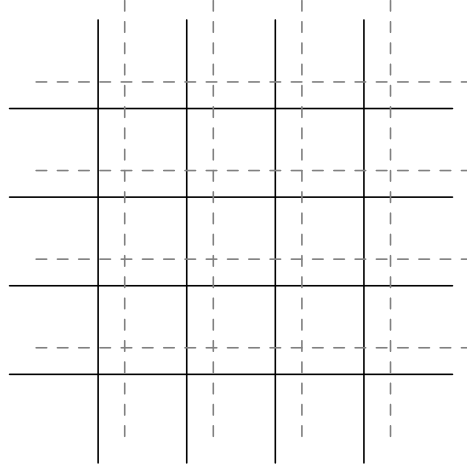


Figure 3.1. Restart with offset to avoid overlapping borders.

**Algorithm 1** Landweber method

---

```

pre-calculate data for fast matrix-vector multiplication
for  $s = 1, 2, \dots, \text{shakes}$  do
  determine offset
  for each segment do
    for  $i = 1, 2, \dots, \text{maxit}$  do
      perform landweber iteration
      check for convergence, continue if not reached
    end for
  end for
end for

```

---

in all areas in-between it is acquired through linear interpolation. This leads to an approximation of  $\mathbf{H}$ , see section 2.2, which is used to iteratively solve equation 2.13 with the Bi-Conjugate Gradient Stabilized (BiCGStab) method [3].

This method[12] uses a variant of the Conjugate Gradient method, BiCGStab [3], to solve equation (2.13). To solve the equation both  $\mathbf{H}\mathbf{v}$  and  $\mathbf{H}^T\mathbf{v}$  are needed but since all PSFs are not known this poses a problem. The known PSFs are represented by known rows in  $\mathbf{H}$  and the rows in between are pixels where the PSF is not known. If the PSF is assumed to behave locally linear the missing rows can be interpolated from the known ones. Below each  $\mathbf{H}_n$  is one known PSF and together with the weight matrices  $\beta_n$  they approximate  $\mathbf{H}$  with

 $\tilde{\mathbf{H}}$ 

$$\tilde{\mathbf{H}} = \beta_1 \mathbf{H}_1 + \beta_2 \mathbf{H}_2 + \dots + \beta_N \mathbf{H}_N, \quad (3.5)$$

$$\sum_{n \in N} \beta_n = \mathbf{I}. \quad (3.6)$$

The image is uniformly split into a number of segments corresponding to the number of known PSFs.

In practice  $\tilde{\mathbf{H}}\mathbf{v}$  is not explicitly calculated since it would be very resource demanding. Instead the structure of  $\mathbf{H}$  is exploited. When dealing with shift-invariant PSFs, which is the case during interpolation,  $\mathbf{H}$  is a Toeplitz matrix and there exists methods for fast multiplication. Therefor the image is split into segments where the PSF is assumed to be locally linear.

Each segment is filtered with the, at most 4, shift in-variant PSFs affecting it and the responses are then interpolated with the corresponding weight matrices, in this case matrices containing coefficients for linear interpolation. See figure 3.2. Finally all segments are put together resulting in  $\tilde{\mathbf{H}}\mathbf{v}$  or  $\tilde{\mathbf{H}}^T\mathbf{v}$ .

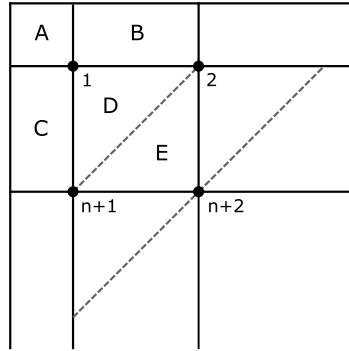


**Figure 3.2.** Upper left corner of the image. A is affected only by the PSF in 1. In B the PSFs in 1 and 2 are linearly interpolated. The same is true in C but with PSFs 1 and  $n + 1$ . D is created by interpolating the three PSFs in 1, 2 and  $n + 1$  and in the same manner E is created from 2,  $n + 1$  and  $n + 2$

Algorithm 2 is the algorithm implemented. After initializing the data for fast matrix-vector multiplication, see appendix A, the equation is solved with a modified BiCGStab.

The interpolation method is the faster of the two methods and each step of the iteration process results in significant changes in the output image. This upside of this is the fast processing time but the downside is that it is harder to keep the method from diverging. This is especially true under noisy conditions.

As far as visual quality is concerned the interpolation method produces slightly sharper images but with slightly more distortions in the corners than the Landweber method. This is fairly obvious in the images blurred by the rotational filter, see section 5.1, where distortions are visible in the corners. One of the causes of these distortions is the shape of the PSF. During restoration of rotational blur the PSF

**Algorithm 2** Simplified BiCGStab

---

```

pre-calculate data for fast matrix-vector multiplication
 $\mathbf{x}^0 = \mathbf{0}$  {initial guess}
 $\mathbf{r}^0 = \mathbf{b} - \mathbf{H}\mathbf{x}^0$ 
 $\tilde{\mathbf{r}} = \mathbf{r}^0$ 
for  $i = 1, 2, \dots, \text{maxit}$  do
   $\rho_{i-1} = \tilde{\mathbf{r}}^T \mathbf{r}^{i-1}$ 
  if  $i = 1$  then
     $\mathbf{p}^i = \mathbf{r}^{i-1}$ 
  else
     $\beta_{i-1} = (\rho_{i-1}/\rho_{i-2})/(\alpha_{i-1}/\omega_{i-1})$ 
     $\mathbf{p}^i = \mathbf{r}^{i-1} + \beta_{i-1}(\mathbf{p}^{i-1} - \omega_{i-1}\mathbf{v}^{i-1})$ 
  end if
   $\mathbf{v}^i = \mathbf{H}\mathbf{p}^i$ 
   $\alpha_i = \rho_{i-1}/\tilde{\mathbf{r}}^T \mathbf{v}^i$ 
   $\mathbf{s} = \mathbf{r}^{i-1} - \alpha_i \mathbf{v}^i$ 
   $\mathbf{t} = \mathbf{H}\mathbf{s}$ 
   $\omega_i = \mathbf{t}^T \mathbf{s} / \mathbf{t}^T \mathbf{t}$ 
   $\mathbf{x}^i = \mathbf{x}^{i-1} + \alpha_i \mathbf{p}^i + \omega_i \mathbf{s}$ 
   $\mathbf{r}^i = \mathbf{s} - \omega_i \mathbf{t}$ 
  check for convergence, continue if convergence not reached
end for

```

---

will cover areas outside of the image thus including unknown image data in the process. To handle this problem the image is padded with suitable data, which may introduce errors in the areas where the PSF is outside of the image.

## 3.4 Performance

Both methods rely on an algorithm for fast matrix-vector multiplication which utilizes the structure of the matrix. This allows for the multiplication between a matrix and a vector to be performed in only  $n \log_2 2n$  complex multiplications, see appendix A.

### 3.4.1 Landweber method

Parts of this method can be implemented in parallel. Each segment is iterated over separately thus can be treated in their own process. This is probably where most performance can be gained since each segment is iterated over around 5 times and each iteration contains 3 time-consuming matrix-vector multiplications. (The representation of  $\mathbf{H}$  for use with the fast multiplication algorithm can be pre-calculated to gain some performance.) On top of this the whole method is restarted up to 3 times. A worst case scenario results in  $45n_s$  matrix-vector multiplications,

where  $n_s$  is the number of segments. As with the interpolation method the number of segments increases the number of elements in each segment decreases which leads to a balancing between few but large segments or many but small.

If the image is split into  $n_s$  segments of dimension  $n \times n$  the total number of complex multiplications for the above typical case of the method is  $\mathcal{O}(90n_s n^2 \log_2(2n^2))$ .

Given an  $m \times m$  image split into  $n_s$  segments the memory demands are  $\mathcal{O}(2m^2)$  for the image and a working copy,  $\mathcal{O}(n_s \frac{m^2}{n_s})$  for the pre-calculated data for the matrix vector algorithm and  $\mathcal{O}(\frac{m^2}{n_s})$  for each process that is working in parallel with a segment. In total for the case of no parallel processing the memory demand is  $\mathcal{O}(3m^2)$ . This is the same amount as the interpolation method uses.

### 3.4.2 Interpolation method

Parts of this method can be performed in parallel using multiple processes working independently from each other. For example the multiplication  $\mathbf{H}\mathbf{v}$ , see section 3.3, since each segment can be treated separately in this step of the method.

Each iteration of BiCGStab contains one  $\mathbf{H}\mathbf{v}$  and one  $\mathbf{H}^T\mathbf{v}$ . Each multiplication consists of 4 fast matrix-vector multiplication per segment this leads to the total number of multiplications being  $8n_s$  per iteration, where  $n_s$  is the number of segments into which the image is split during processing. As the number of segments increases the number of elements in each segment decreases which leads to a balancing between few but large segments or many but small.

If the image is split into  $n_s$  segments of size  $n \times n$  the matrix-vector multiplications are between a  $n^2 \times n^2$  matrix and a  $n^2 \times 1$  vector. The total number of complex multiplications per iteration is  $\mathcal{O}(16n_s n^2 \log_2(2n^2))$ .

Given an  $m \times m$  image split into  $n_s$  segments the memory demands are  $\mathcal{O}(2m^2)$  for the image and a working copy,  $\mathcal{O}(n_s \frac{m^2}{n_s})$  for the pre-calculated data for the matrix vector algorithm and  $\mathcal{O}(\frac{m^2}{n_s})$  for each process that is working in parallel with a segment. In total for the case of no parallel processing the memory demand is  $\mathcal{O}(3m^2)$ .

## 3.5 Limitations

To keep the implementations of the methods on a reasonable level they are limited to some extent. The most important limitations are the following:

- The images must be square.
- The number of estimated PSFs are constrained by the image size. The number of filters must divide the image into equally-sized segments. With an image of size  $256 \times 256$  the number of PSFs can be  $2^2, 4^2, 8^2 \dots$
- The methods are not optimized for execution speed.

- The estimated PSFs are assumed to be spaced equidistantly over the image plane
- The automatic stopping criterion are not optimal in the implementations of the methods in this report. For the interpolation method it is too restrictive and for the Landweber method it is too loose. The main goal of this report is to evaluate the performance of the methods ability to restore images, autonomy is not a demand.





## Chapter 4

# Evaluation

The goal of the image capturing is to interpret the contents of the image manually by a human operator and/or automatically by software based methods. The interpretation can only be successful if the image quality is high enough. Exactly what quality measures are relevant will depend on the application, as well as the interpreter. In this report however the final use is not specified thus the methods must be evaluated in several different ways.

The results produced by the restoration algorithms were evaluated both subjectively and objectively. The subjective evaluation consisted of a visual examination of each image as it was restored, judging when the best possible result had been reached. This is a good method when optimizing the output image for human observers but not necessarily when the images are to be further processed automatically. One of the most important differences being that the human vision system is much more noise tolerant than most automatic methods.

### 4.1 Test images

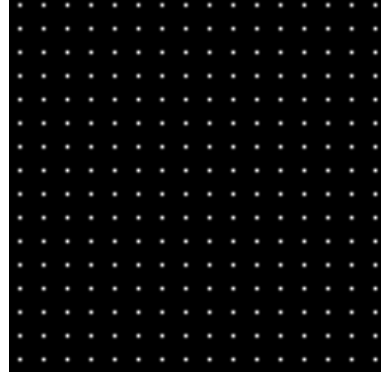
Two synthetic and one natural image were used during evaluation, each for a specific purpose.

- **softdots\_256** This image consists of gaussians placed evenly in the image. It represents a number of point-shaped objects. See figure 4.1.
- **sat\_256** This is a satellite image of an area with buildings, roads and trees and it was chosen to evaluate the methods visually. The image contains a mix of small objects, sharp edges and smooth structures which makes it a good overall image for evaluation purposes. It is interesting to study since it is a “natural” image. See figure 4.1.
- **dotring\_256** This is an image specially designed for use with one of the evaluation methods, see section 4.3. 25 Gaussian bells with  $\sigma = 2$  are placed in a circle around the center of the image. See figure 4.1.

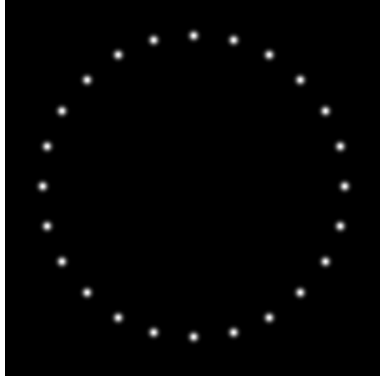
All images used have the amplitude range of  $[0, 1]$ .



(a)



(b)



(c)

**Figure 4.1.** (a) sat\_256 and (b) softdots\_256 (c) dotring\_256

## 4.2 Generation of synthetic blurs

To evaluate the restoration methods they were tested on both synthetic and real images, both types blurred synthetically. The use of synthetic blur is motivated by the need to know the exact PSF used during blurring to be able to evaluate the performance of the methods after restoration. Using synthetic images allows for specific measurements of performance.

Application of the synthetic blur was done by traversing the images pixel by pixel and applying the local estimate of the PSF simulated. To avoid edge effects a larger image was used during blurring and the final image was cut out.

- **Radial blur.** Synthetisation of the zoom-effect that arises when the imaging system is moving at high speed along the Line of Sight(LOS) during exposure.

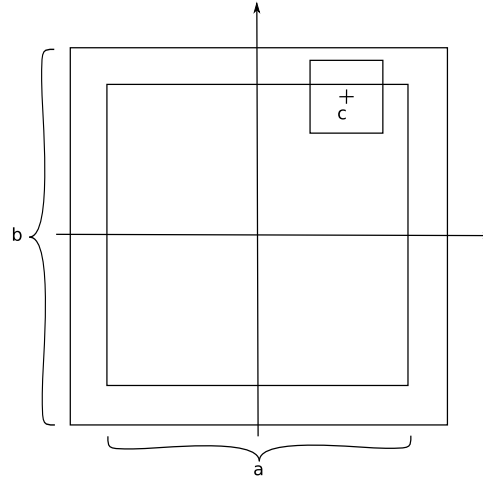


**Figure 4.2.** Image during application of synthetic blur. (a) is the image size, (b) is the image size with padding and (c) is the size of the PSF as it moves around the image during application.

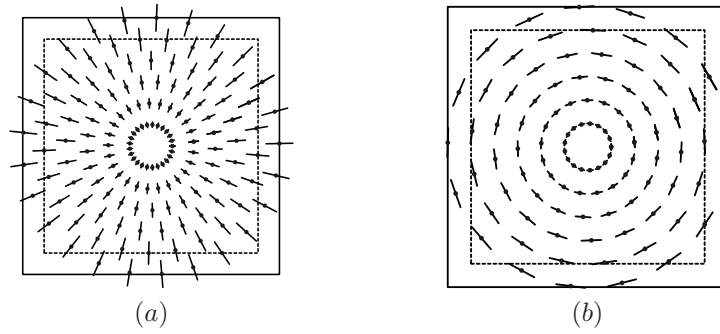


**Figure 4.3.** A few kernels estimating (a) radial and (b) rotational blur

A similar blur can also arise from the lens system of the imaging system and is then known as sagittal astigmatism. Locally the kernel is estimated with a 1-D motion blur parallel to the radius  $r$  and a length that varies as  $\gamma r$ , where  $\gamma$  is defined as the blur size. For more details see figure 4.3.

- **Rotational blur.** Synthetisation of the rotation-effect that arises when the camera is mounted on a rotating platform. This blur is also similar to the optical aberration called tangential astigmatism. Locally the kernel is estimated with a 1-D motion blur perpendicular to the radius  $r$  and has a length that varies as  $\gamma r$ , where  $\gamma$  is defined as the blur size. For more details see figure 4.3.
- **Gaussian blur.** Synthetisation of spherical blur that approximates the effect

of the lens system in the imaging system. It is also similar to out-of-focus blur. Out-of-focus blur is actually given by the Airy function [7] but can in most cases be well approximated by a gaussian function. It is syntheticated by radially varying gaussian blur where the variance of the kernel varies with the radius  $r$  as  $\sigma^2 = \gamma(0.1 + r)$ .  $\gamma$  is an amplification parameter to control the amount of blur similar to the size of the blur above.

- **Coma.** Synthetisation of coma that arises in the lens system of the imaging system. The PSF is simulated by using pre-calculated kernels and interpolating them over the image. The kernels span the area  $r = [0, 1]$  and are rotationally invariant. Because of the work involved in calculating coma PSFs only 16 are used during interpolation. Pre-calculated kernels are used because of the large amount of time it takes to calculate every needed kernel. The kernels were calculated in Zemax, a software tool for optical simulations.

Since all blurs vary over the image the “blur size” must be defined. For rotational and radial blur it is defined as the length of the 1-D blur at  $r = 1$ . For the gaussian blur the size is defined as the variance of the kernels at  $r = 1$  minus the DC-component of 0.1. These definitions of blur size leads to the blur applied being larger than the specified size in the corners of the image. This in turn leads to distortions appearing in the corners during restoration. The distortions would normally appear anyway but will generally be larger than expected if the definition of blur size is not taken into account.

When estimating the blur in the synthetic images prior to restoration the same synthetic model of the blur is used as when the blur was applied. This is important when evaluating the restoration methods since this way the estimation of the blur will not introduce any errors. How the restoration quality is affected by the precision of the estimation is interesting and is studied separately.

### 4.3 Evaluation methods

The objective evaluation was performed by means of automatic restoration and measurement using a number of measurements described below. The measurements used are SNR and ME which are both commonly used in the literature. The task of finding objective measurements that covers all aspects of image restoration is nearly impossible and lies beyond the scope of this report.

SNR and ME are useful, especially since they are commonly used, thus allows for comparison between methods in literature.

Let  $o(n)$  be the discrete object scene represented by a vector with  $N$  pixels and let  $i(n)$  be the blurred image represented by a vector with  $N$  pixels. Define  $\mu_0$  as the mean pixel value for  $o(n)$ .

$$\text{SNR} = 10 \log \left( \frac{\sigma_{\text{object}}^2}{\sigma_{\text{MSE}}^2} \right) \quad (4.1)$$

where  $\sigma_{\text{object}}^2$  and  $\sigma_{\text{MSE}}^2$  are defined as

$$\sigma_{\text{object}}^2 = \frac{1}{N} \sum_{n \in N} |o(n) - \mu_o|^2 \quad (4.2)$$

$$\sigma_{\text{MSE}}^2 = \frac{1}{N} \sum_{n \in N} |o(n) - i(n)|^2 \quad (4.3)$$

and

$$\text{ME} = \frac{1}{N} \sum_{n \in N} |o(n) - i(n)| \quad (4.4)$$

One of the advantages of using automatic measurements like ME and SNR is their speed. Images can be batch-processed and steps can be taken to allow for statistically significant results. The drawback is that the results can be hard to interpret. One visually appealing result may show up as a very poor one when judged by SNR or ME. Another advantage is the wide spread use of SNR and ME. Although blunt they give a good indication of the general trends that follows varying parameters like blur, noise and method parameters.

Presented in the plots in chapter 5 is ME in the measured image divided by the ME in the blurred image with noise applied. This way the measure can be compared with the blurred image to see if there has been any improvement.

Another automatic evaluation method was used to study the performance of the restoration methods in different parts of an image. This method is somewhat experimental but proves to be a generally good measure of local improvement. The goal of the measure is to estimate the gain in detail at a certain distance from the center of the image. This is interesting because the blurs used during evaluation varies radially. For this the dotring\_256 image was used. The image is specifically designed for this measure with Gaussian bells placed in a circle around the image center. The measure is calculated as an average over all Gaussian bells. Since the standard deviation of the Gaussian bells before degradation is known, see section 4.1, the standard deviation after restoration can be compared to this to create a relative measure of improvement. The standard deviation after degradation can be estimated by measuring the half-height full width of the bells. The half-height is defined as half of the maximum height at the peak.

Manipulating the expression for a Gaussian results in a simple expression to calculate the standard deviation from the half-height full-width.

$$f(x) = Ce^{-\frac{x^2}{2\sigma^2}} \quad (4.5)$$

Let  $h$  be the half-height.

$$\frac{1}{2}C = Ce^{-\frac{h^2}{2\sigma^2}} \quad (4.6)$$

$$\ln \frac{1}{2} = -\frac{h^2}{2\sigma^2} \quad (4.7)$$

$$h^2 = 2 \ln 2 \sigma^2 \quad (4.8)$$

$l_h$  is the full-width at the half-height.

$$l_h \approx 2.355\sigma \quad (4.9)$$

In the case of Gaussian blur the standard deviation in the blurred image,  $\sigma_{\text{blurred}}$  can even be calculated theoretically as

$$\sigma_{\text{blurred}} = \sqrt{\sigma_{\text{object}}^2 + \sigma_{\text{PSF}}^2} \quad (4.10)$$

where  $\sigma_{\text{PSF}}$  denotes the variance of the PSF applied.

The final measure is defined as

$$\Delta\sigma = \frac{\sigma_{\text{measured}}}{\sigma_{\text{objnoise}}} \quad (4.11)$$

where  $\sigma_{\text{measured}}$  is the measured standard deviation from a restored or blurred image. *objnoise* denotes the original image with only noise applied.

## Chapter 5

# Results

The methods were first visually evaluated to determine suitable parameters for batch testing. Since no per-restoration optimization was to be performed the parameters had to be constant but still perform well at many different levels of blur and noise. This lead them to be a bit restrictive as far as quality of the restoration was concerned. They were finally chosen to the lowest value that produced visually good results.

It turned out that for the interpolation method the maximum number of iterations suitable was 5.

For the Landweber method the maximum number of iterations was 15 for all blurs tested except Gaussian blur. The method turned out to be rather sensitive to the level of noise. For the Gaussian blur the maximum number of iterations was chosen to be 5. The number of shakes, see section 3.2 for definition of the shakes parameter, was chosen to 3 for all blurs.

To avoid random anomalies in the measured data due to the random noise each test was repeated several times to produce an average measurement. For the interpolation method each test was repeated 10 times and for the Landweber method they were repeated 5 times. The lower number for Landweber was because it takes significantly longer time to restore an image than the interpolation method.

### 5.1 Visual Comparison

This section compares the two restoration methods visually. As a reference a comparison with a direct inverse filter was also made, in this case the Wiener Filter.

Since the Wiener filter only uses one shift-invariant PSF during restoration it had to be chosen with care. When restoring the varying Gaussian blur the PSF was picked at  $2/3$  from the center of the image.

The rotational and radial filters are even more problematic for the Wiener filter since they are directional, one PSF of the estimated ones can't be chosen since it

is very different from the filters used in other parts of the image. Thus, a Gaussian filter was used to act as a kind of sharpening filter.

Comparison was also made with a shift-invariant PSF to illustrate that direct inversion filters can be quite powerful and to see how the evaluated methods compare to them.

### 5.1.1 Shift-invariant PSF

The methods was also compared to the wiener filtering when the test image was blurred by a shift-invariant filter. Gaussian blur with standard deviation 1.1 was used during testing. The results can be viewed in figures 5.1 and 5.2.

There are no great differences between the restored images from the different methods. The images produced by the Landweber method are a bit more blurry but that is about it. This indicates that, if used on shift-invariant blur, the evaluated shift-variant methods will perform well with the Wiener filter as a reference.



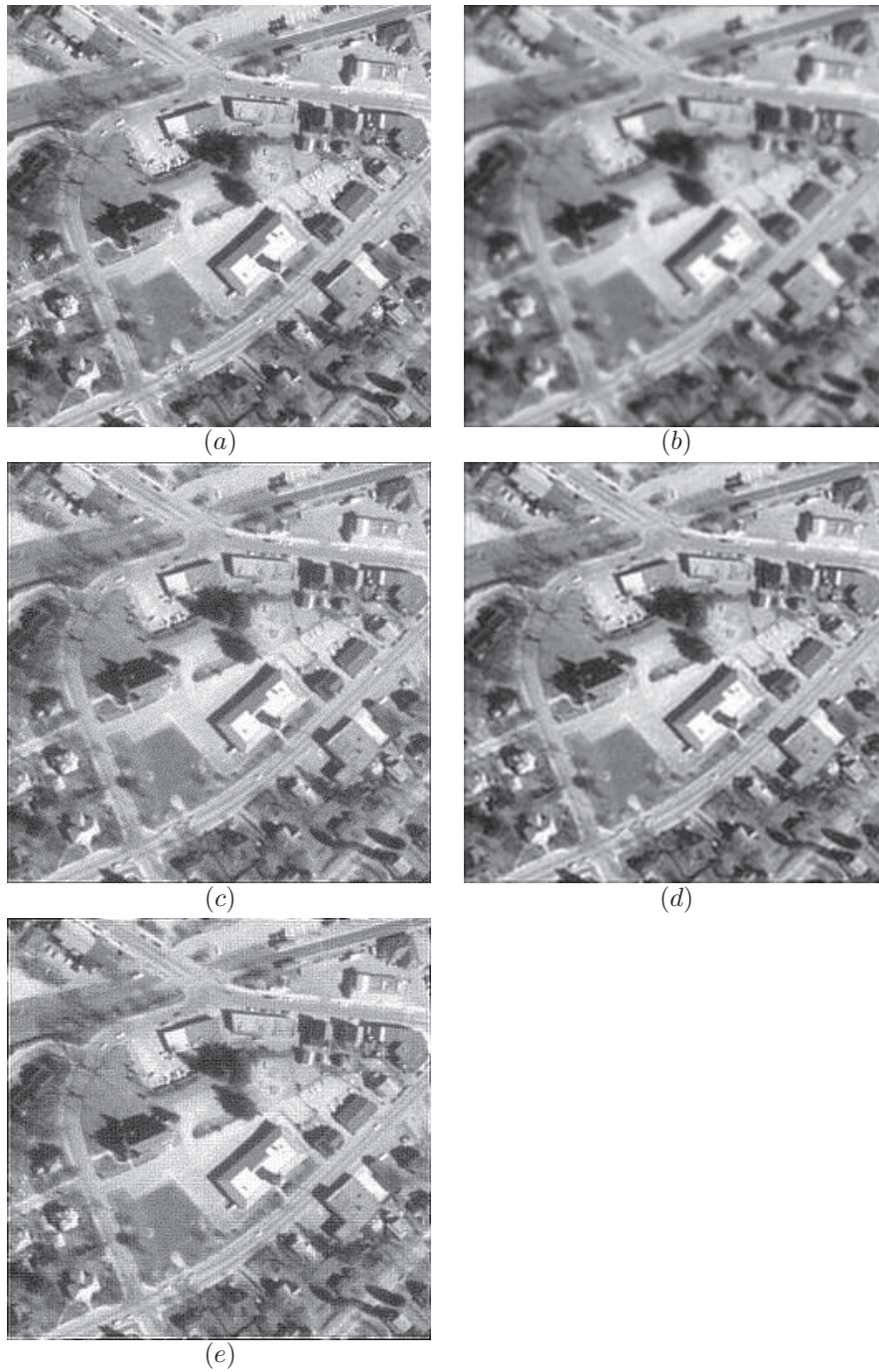


**Figure 5.1.** (a) is the original image. (b) has been blurred by shift-invariant Gaussian blur with  $\sigma = 1.1$  and noise has been added so that SNR=30 dB. (c) is restored with the interpolation method and (d) is restored with the Landweber method. (e) is restored with the wiener filter.

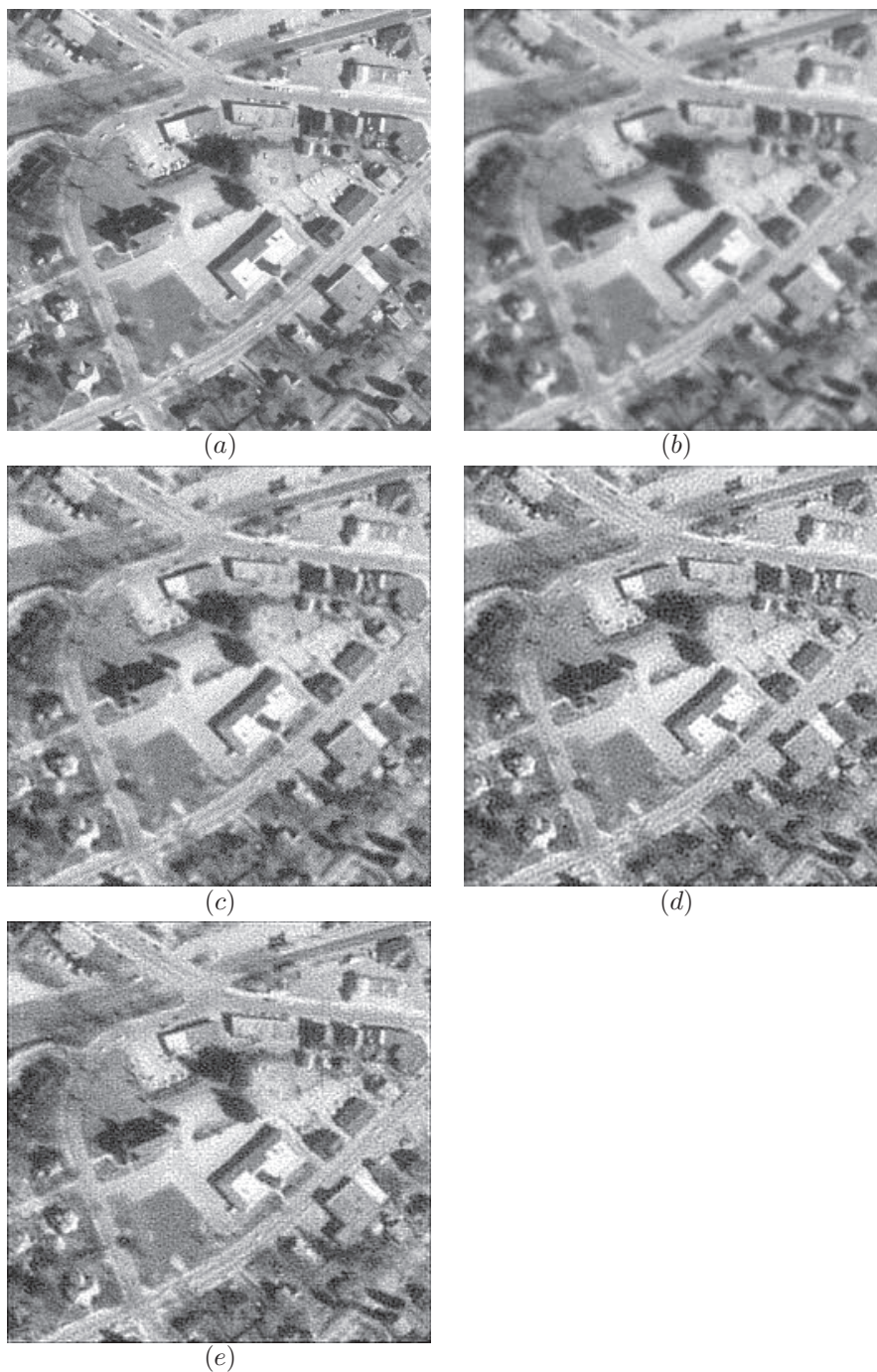


**Figure 5.2.** (a) is the original image. (b) has been blurred by shift-invariant Gaussian blur with  $\sigma = 1.1$  and noise has been added so that SNR=15 dB. (c) is restored with the interpolation method and (d) is restored with the Landweber method. (e) is restored with the wiener filter.

### 5.1.2 Shift-variant PSF

The wiener filter cannot handle shift-variant blur, at least not directly. When dealing with rotational or zoom blur for example, the image can be transformed to plane-polar coordinates which results in a shift-invariant PSF. The restoration can then be performed with a direct inverse method such as the wiener filter [8]. However, if there is more than one blur affecting the image the transformed image may still contain a shift-variant PSF. If an image is affected by rotational blur and a horizontal sweep the latter PSF will result in a shift-variant PSF in plane-polar coordinates.

In figure 5.3 results on the natural image are compared between the two methods when the image is blurred with rotational blur. Presented are the original image, the blurred image with noise (SNR=30dB) and the restored images. The noise is hardly visible in the original image but still causes distortion during restoration.

The blockiness produced by the Landweber method is slightly visible, more pronounced towards the edges. Some blur remains in the Landweber image leading to the interpolation image appearing significantly sharper. Both images have distortion in the corners, the interpolation image perhaps a bit more.

Overall the interpolation method performs better on this image as far as visual quality is concerned.

In figure 5.4 the same comparison is done as above but with noise SNR at 15dB. The restored images are very noisy. The interpolation method had to be stopped after only 1 iteration to limit the noise thus the image is also very blurry. None of the methods produce good results but the images restored by the interpolation method are less distorted although more blurry.

Figure 5.5 compares the methods when they are restoring images blurred by the radial blur. The two shift-variant methods produce good results and the increase in visual quality is noticeable. The Landweber methods suffers from distortions around the edges. This is because of the way the image is split during restoration.

In figure 5.6 the same comparison is done as above but with noise SNR at 15dB. The restored images are very noisy. The interpolation method had to be stopped after only 2 iterations to limit the noise thus the image is also very blurry. None of the methods produce good results but the images restored by the interpolation method are less distorted although more blurry.

In figure 5.7 results on the natural image are compared between the two methods and wiener filtering when blurred by shift-variant Gaussian blur. Presented are the original image, the blurred image with noise (SNR=30dB) and the restored images. The noise is hardly visible but still causes distortion during restoration. The interpolation methods shows signs of distortion in the corners of the image while the Landweber method is free of such error. Overall the interpolation method performs better on this image as far as visual quality is concerned.

In figure 5.8 the same comparison is done as above but with noise SNR at 15 dB. The restored images are very noisy. The interpolation method had to be stopped after only 2 iterations to limit the noise thus the image is also very blurry. None of the methods produce good results but the images restored by the interpolation



method are less distorted although more blurry.

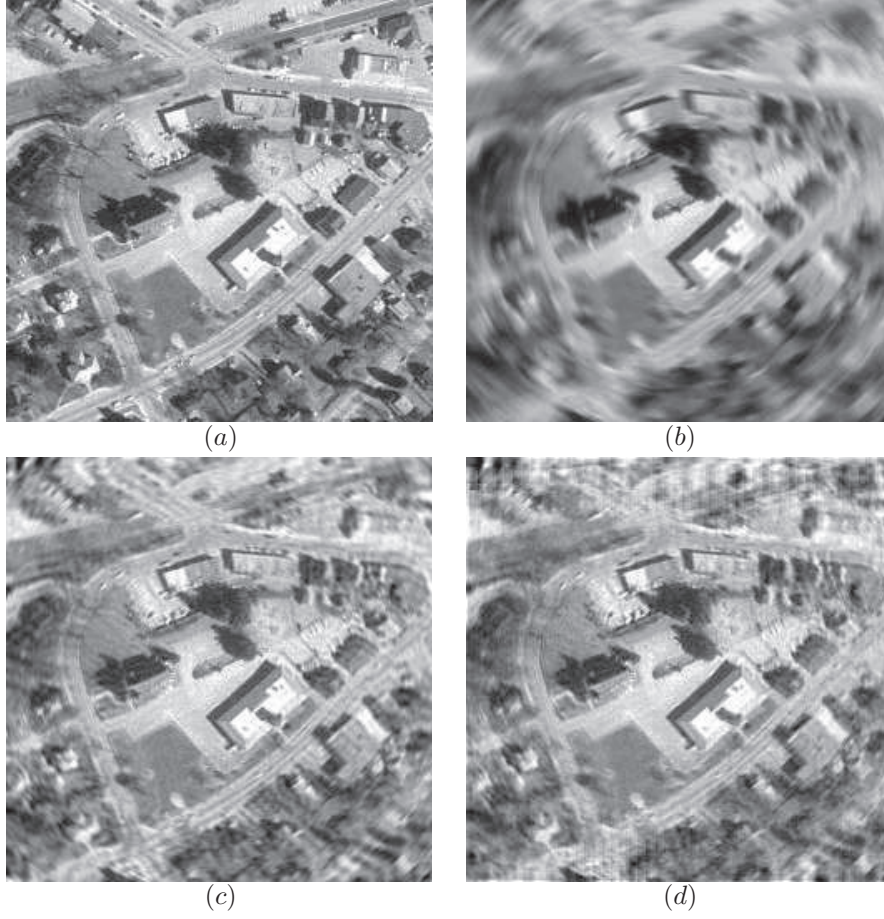


**Figure 5.3.** (a) is the original image. (b) has been blurred by rotational blur with blur size 13 and noise has been added so that SNR=30 dB. (c) is restored with the interpolation method and (d) is restored with the Landweber method.

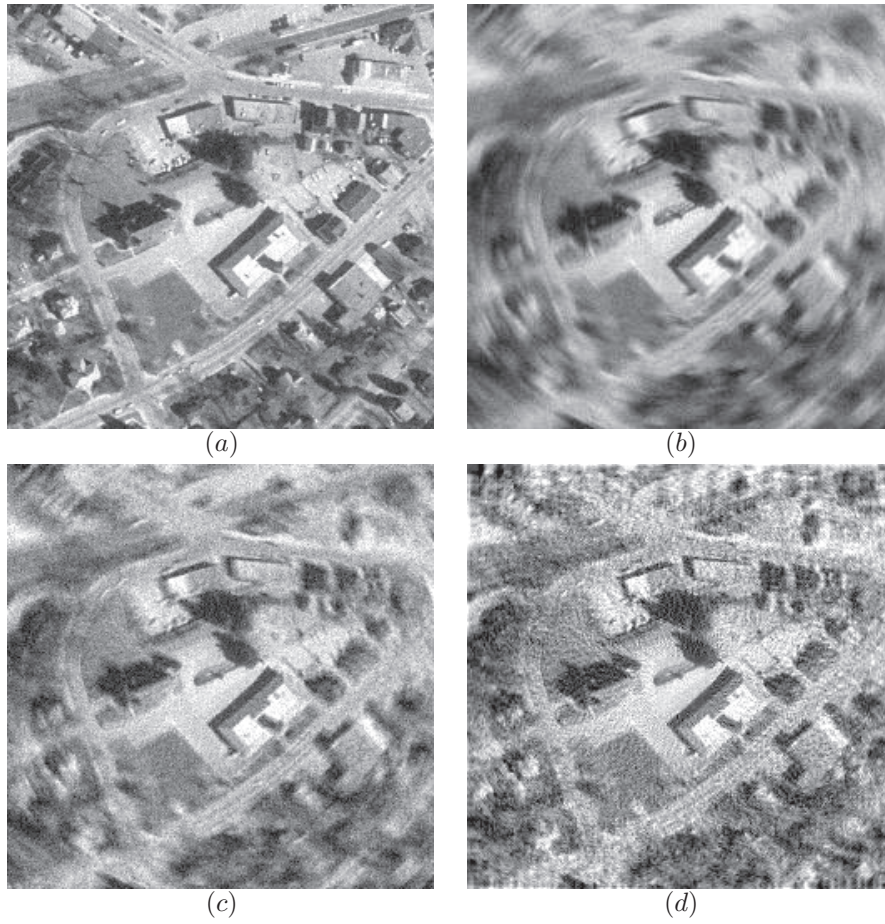


**Figure 5.4.** (a) is the original image. (b) has been blurred by rotational blur with blur size 13 and noise has been added so that SNR=15 dB. (c) is restored with the interpolation method and (d) is restored with the Landweber method.

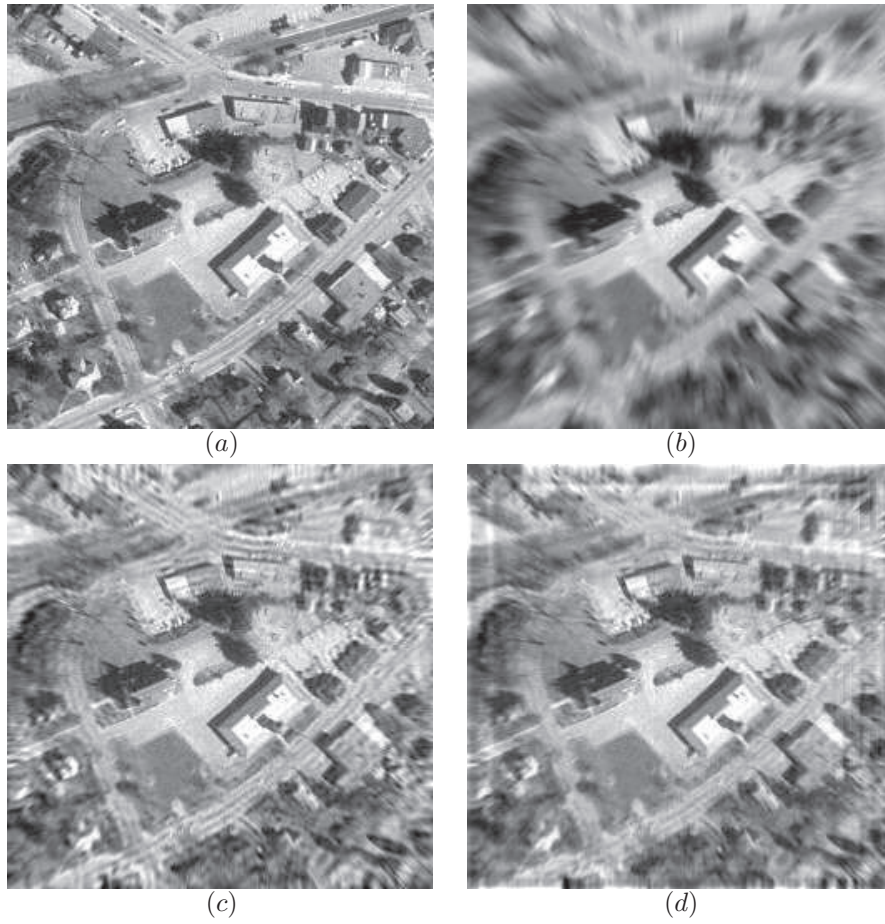


**Figure 5.5.** (a) is the original image. (b) has been blurred by radial blur with blur size 13 and noise has been added so that SNR=30 dB. (c) is restored with the interpolation method and (d) is restored with the Landweber method.



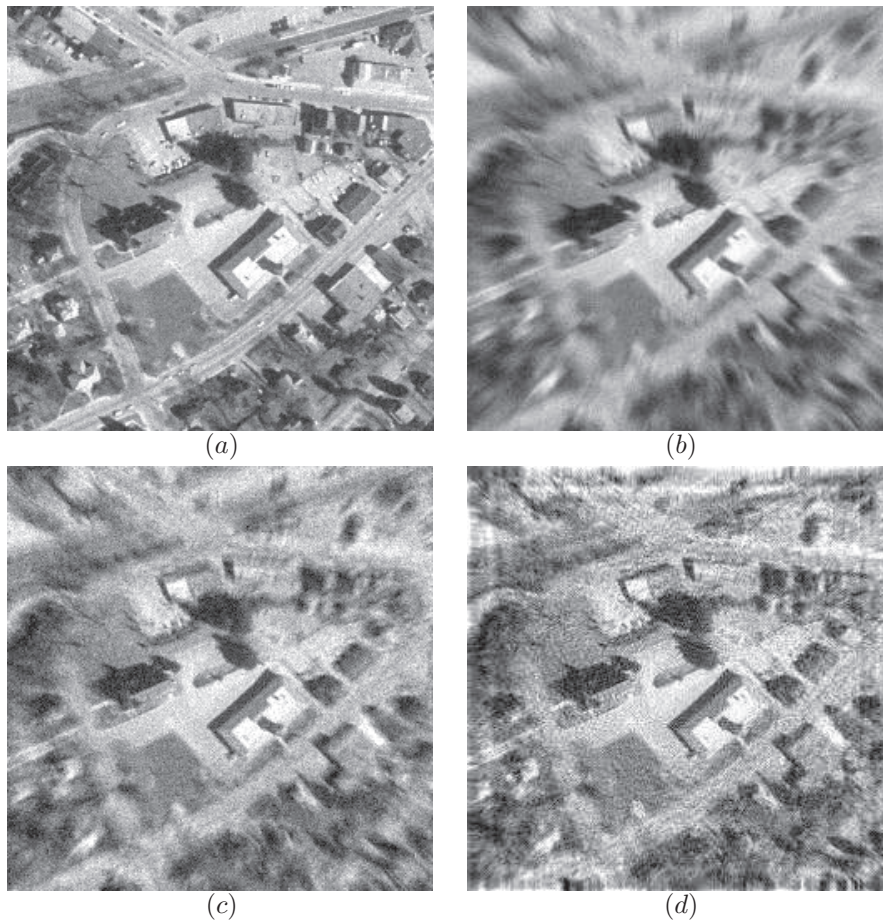


**Figure 5.6.** (a) is the original image. (b) has been blurred by radial blur with blur size 13 and noise has been added so that SNR=15 dB. (c) is restored with the interpolation method and (d) is restored with the Landweber method.

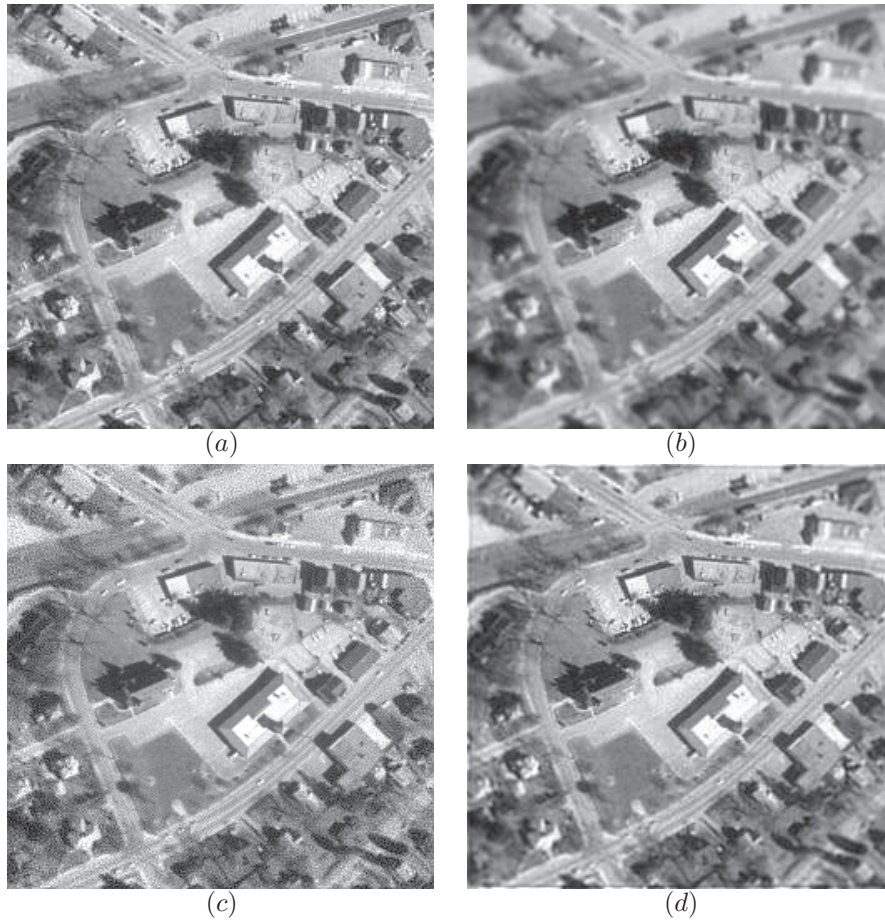


**Figure 5.7.** (a) is the original image. (b) has been blurred by variant Gaussian blur with blur size 13 and noise has been added so that SNR=30 dB. (c) is restored with the interpolation method and (d) is restored with the Landweber method.



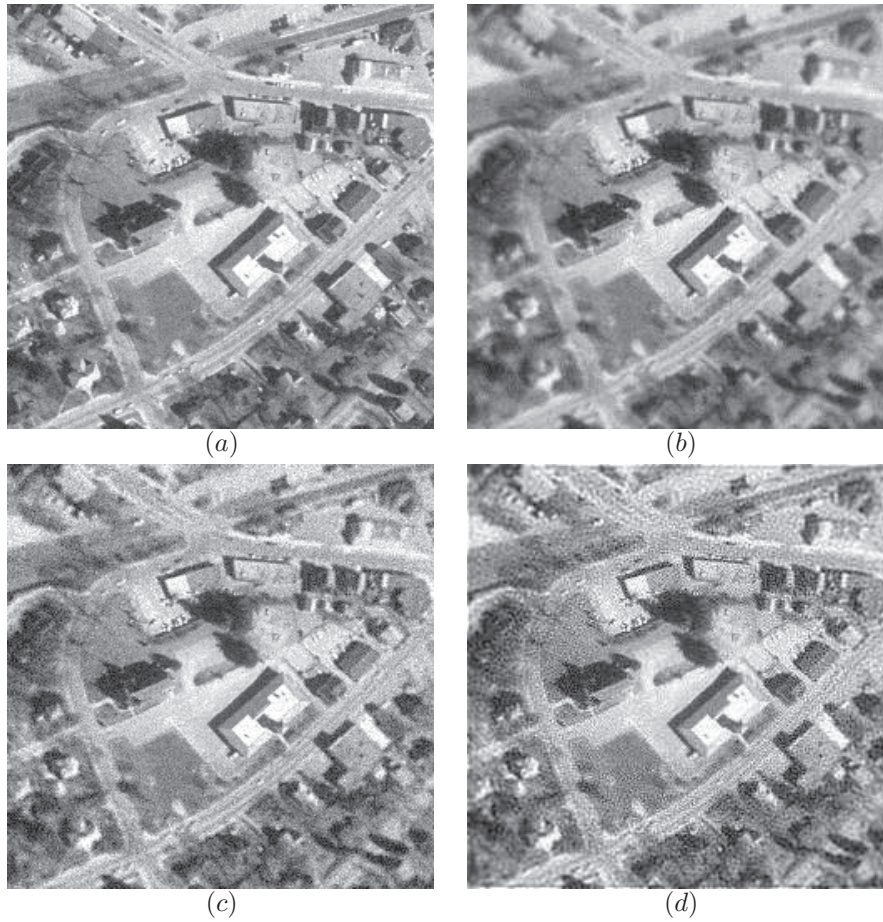


**Figure 5.8.** (a) is the original image. (b) has been blurred by variant Gaussian blur with blur size 13 and noise has been added so that SNR=15 dB. (c) is restored with the interpolation method and (d) is restored with the Landweber method.

## 5.2 Varying blur size

The two restoration methods were tested to see how well they perform at different amounts of blur, trying to find a limit to when they cease to produce useful output. During testing the noise level was constant at 30dB while the blur size varied. For rotational- and radial blur it varied between 5 and 21 and for the Gaussian blur the size varied between 0.25 and 1.75.

Presented in figure 5.9 are the results from testing the two restoration methods with respect to the size of the blur in the blurred image. As a reference, measurements on the images with only blur and noise applied are included.

For both methods SNR decreases as the blur size increases. This is expected since the method is unable to handle fast varying PSFs. When the blur size of the synthetic blurs is large, the blurs will also vary fast over the image.

Both ME and SNR indicates that the interpolation method is useful for all blur sizes tested but that it works best for small blurs, between 5 and 15 for rotational and radial blurs. The interpolation method appears to have problems restoring Gaussian blur in the natural image but this is not really the case which is apparent in the visual evaluation, see section 5.1. Overall the interpolation methods seems to reduce the ME while the Landweber method always increases it.

With the natural image the interpolation methods performs better than the Landweber method but the Landweber method appears to perform better with the soft dots image.

The Landweber method shows the same basic behavior as the interpolation method but appears to be more sensitive to the blur size. Although it outperforms the interpolation method when restoring the softdots image SNR decreases quickly towards levels equal to those of the interpolation method. SNR for the Landweber method dips below the reference at blur size 15 for the natural image.

Both methods seems to be able to deal with all sizes of Gaussian blur since SNR is above the reference for all sizes. The interpolation method performs best with respect to ME.

The  $\sigma$  plot in figure 5.10 indicate that both methods work for the tested blurs but that the interpolation method is somewhat better. The restoration methods are able to restore the Gaussian in the test image. As the blur size increases and  $\sigma$  for the blurred image rises quickly,  $\sigma$  for the two methods rises slowly. This would indicate that there is a limit to how close to the original sharpness the restored sharpness can come.

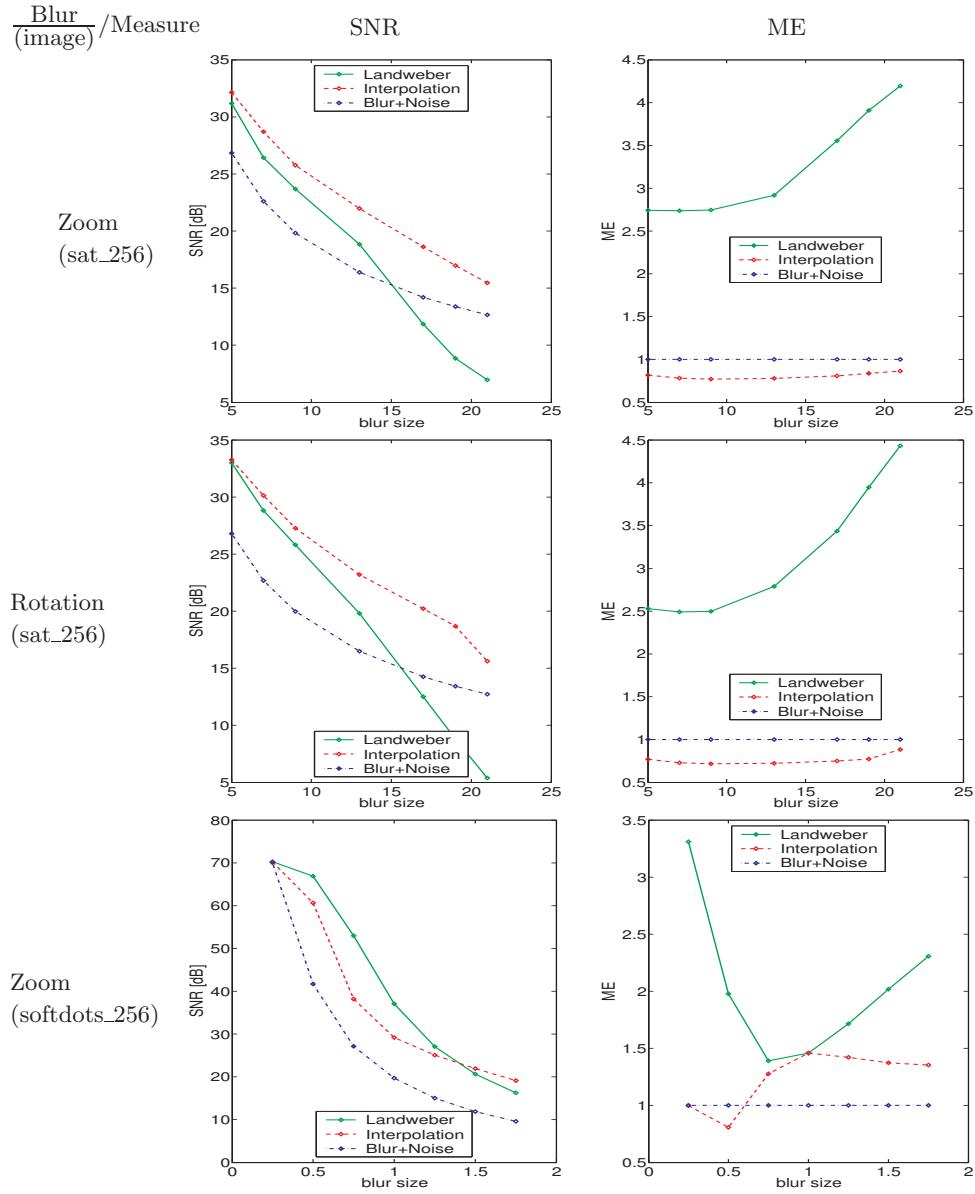


**Figure 5.9.** SNR and ME per pixel as a function of the blur size. The noise level in the blurred image was held constant at SNR=30 dB. For the zoom and rotation blurs the blur size varied from 5 to 21. For the Gaussian blur the blur size varied from 0.25 to 1.75. Presented are the measurements on the sat\_256 image for zoom and rotational blur and on the softdots image for the Gaussian blur.

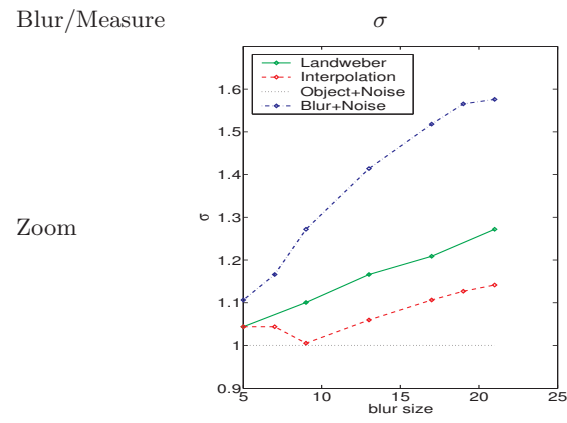


**Figure 5.10.** Change in variance of the Gaussians in the test-image as a function of the blur size.

### 5.3 Varying noise

The two restoration methods were tested with varying noise level to see how sensitive they are to noise. This is interesting since it results in demands on the level of noise in the working environment of the methods. The blur size was constant in all images while the noise level varied. The noise variance was chosen so that the SNR in the blurred image varied between 5 and 40dB with increments of 5dB. For rotational and radial blur the blur size was 13 and the Gaussian blur size was 1, for more details on the blurs see section 4.2.

Presented in figure 5.11 are the results from testing the two restoration methods with respect to the amount of noise in the blurred image.

As expected SNR decreases and ME increases as the noise SNR decreases. A “knee” is visible in the plots at 20-25dB in the natural image and at 10-15dB in the softdot image.

Both the Landweber and the interpolation method perform similarly but as seen when testing varying blur size the different methods shows certain trends for certain combinations of blur and image. The Landweber methods seems to be better at restoring Gaussian blur and especially the artificial image containing Gaussians.

The  $\sigma$  plots shows somewhat random values at high noise levels (low SNR in blurred image) but this is not strange since both methods are quite noise sensitive as seen above. The curves stabilize at around SNR=20 dB which appears to be the limit of noise tolerance.

The parameters for the Landweber method was adjusted. For radial and rotational blur the maximum number of iterations was 15 and for Gaussian blur it was 5. The number of shakes, see Section 3.2, was 3 for all blurs.

Aside from the radial blur both SNR and ME behaves as expected. The Landweber method seems to have generally higher SNR and lower ME. For the softdots\_256 image the SNR is above the reference for all noise levels which would indicate improvement in quality regardless of the investigated noise level. Although the improvement decreases with increasing noise level.

With the natural image the curves flatten out after about 25 dB and remains constant. This is probably because of the distortion that occurs in the corners of the image during restoration. For the softdots image the curves doesn't flatten out as much, mainly because the corners remain largely intact during restoration. This is because the padding that is used during restoration works better with the softdots image than with the natural image.

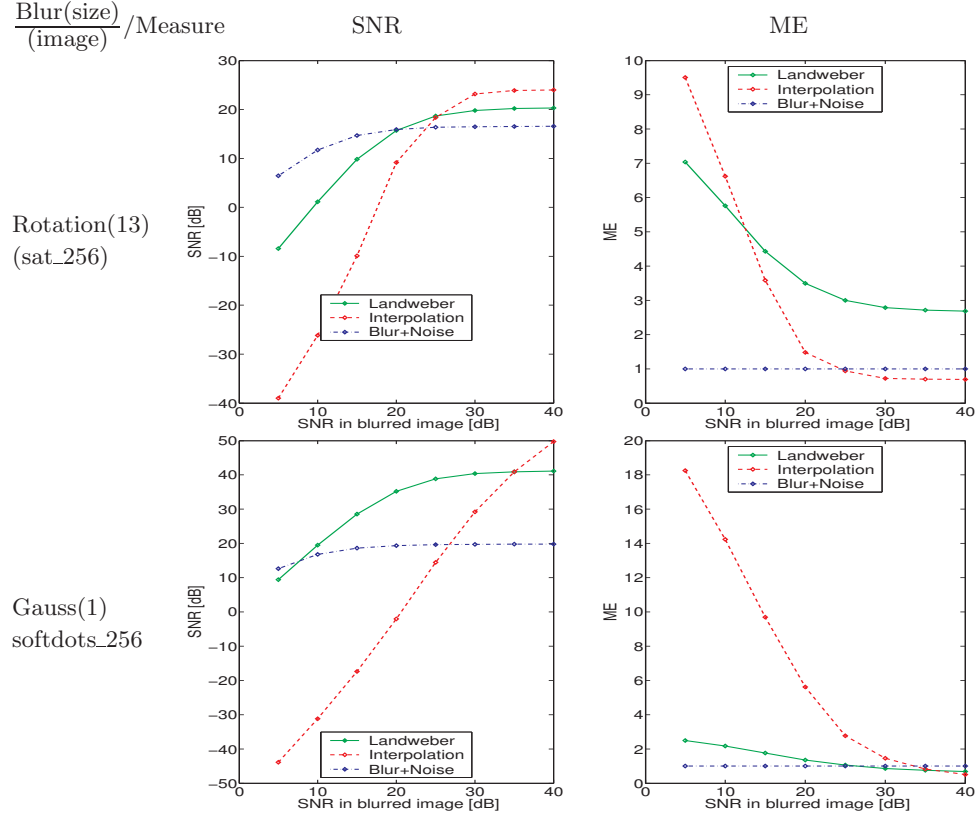


**Figure 5.11.** SNR and ME per pixel as a function of the noise level in restoration of the blurred images. The noise level was measured as SNR in the blurred image. The rotation and zoom blur sizes were 13 and the Gaussian blur size was 1. Presented are the results of measurement on the sat\_256 image for rotational blur and the softdots image for Gaussian blur.

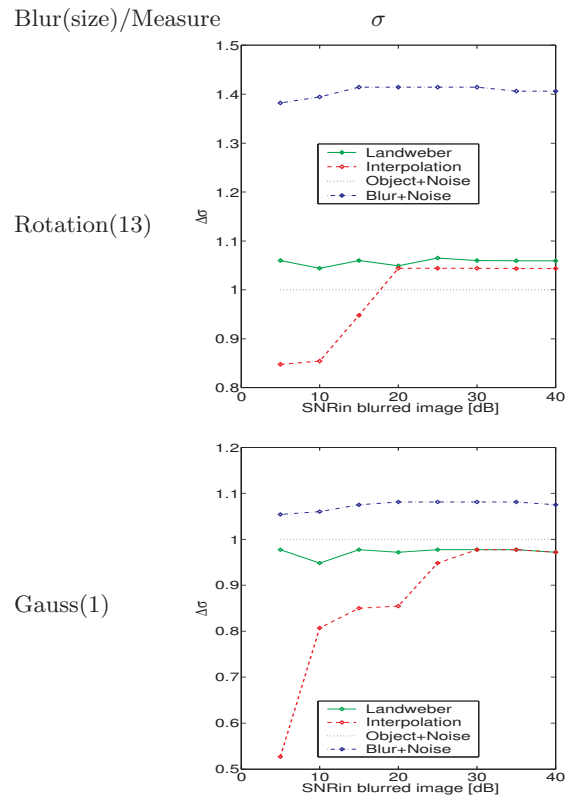


**Figure 5.12.** Change in variance of the Gaussians in the test-image as a function of the noise level.

## 5.4 Varying PSF estimate

The two restoration methods were tested to see how sensitive they are to errors in the PSF estimate. This is interesting since it places demands on the algorithms used for estimating the PSF to be used during restoration. The images were blurred with blur size 13 for rotation and radial blur and blur size 1 for Gaussian blur. During testing the noise level was constant at 30dB. During restoration the estimated blur size varied between  $\pm 20\%$ .

Presented in figure 5.13 are SNR and ME for the restored images and also the SNR and ME measures for the images with only blur and noise applied as a reference. If the restoration has improved the image quality the SNR for the two evaluated methods are expected to stay above the reference while the ME for the methods should be below the reference.

As the deviation from the correct PSF increases SNR decreases and ME increases. Certain trends are visible.

When dealing with natural images or “kind” (in this case Gaussian) PSFs it appears to be better to underestimate the size of the blur. This is because the number of iterations was constant and the fact that small PSFs results in small changes during restoration. Leaving the method to iterate on an image blurred by a larger PSF makes the image somewhat better. When applying one of the methods with the Gaussian PSF it acts as a kind of sharpening filter, this is true for radial and rotational too but for them the sharpening is directional. If the PSF is overestimated the restoration process diverges if not stopped early, the method over-compensates the smaller PSF introducing errors.

Using SNR to measure the quality of natural images is a difficult task since even images with visible artifacts and distortions can have the same SNR as a visibly better-looking image.

In the softdots image opposite trends are visible. For such images it seems to be slightly better to over-estimate the PSF. Although the statement about “kind” PSFs is still true there is a difference when dealing with rotational- and radial blur.

The Landweber method shows the same trends as the interpolation method but with slightly less steep curves suggesting a more error tolerant behavior. Both methods seems to be able to work with errors in PSF estimation, at least as long as the error only lies in the size of the blur.

The  $\sigma$  measure shows that when the blur size lies within  $\pm 10\%$  of the true size both method performs their best, see figure 5.14. The interpolation method is better than the Landweber method in the  $\pm 10\%$  interval but only slightly better outside of it.



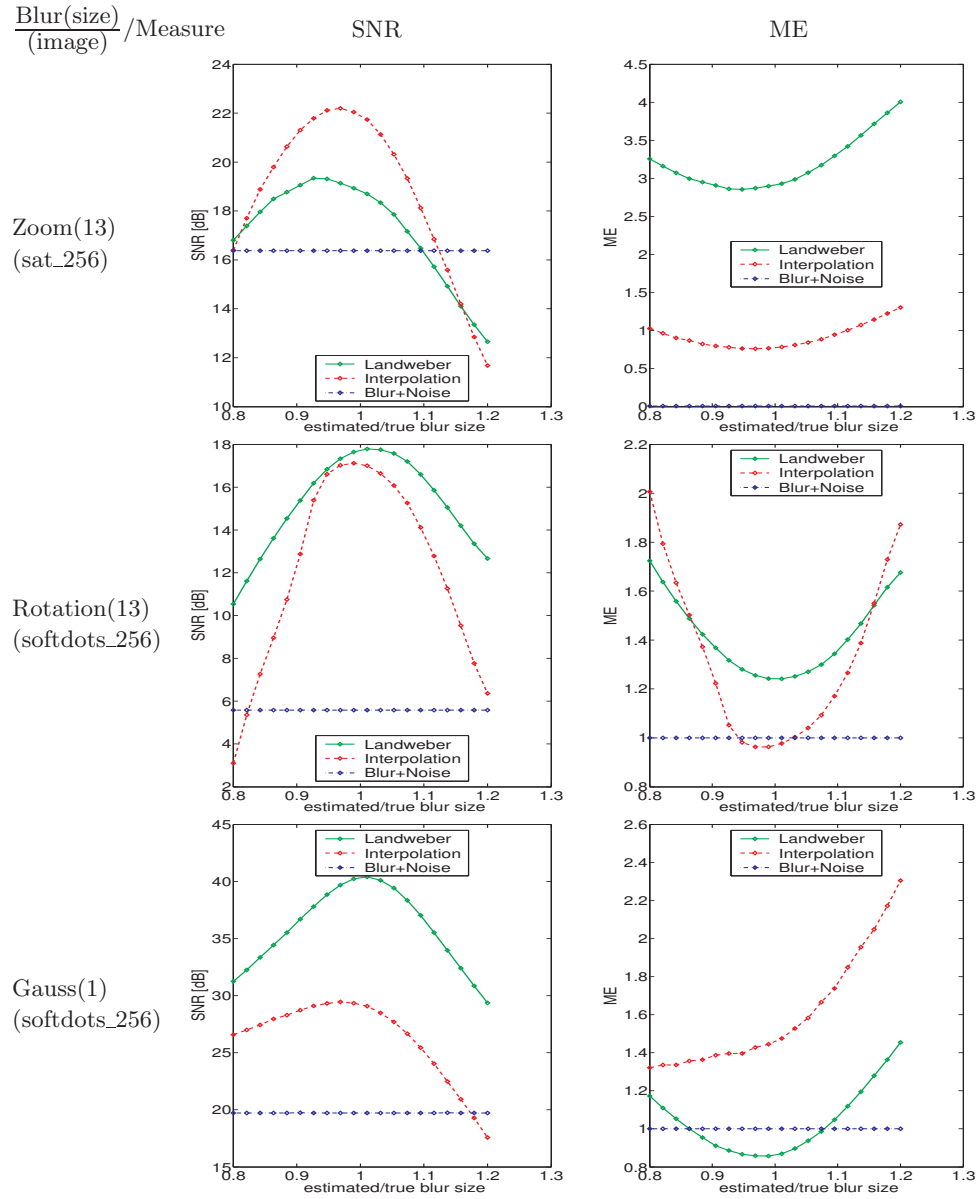


**Figure 5.13.** SNR and ME per pixel as a function of the accuracy of the PSF-estimate in restoration of various blurs. The noise level was constant at SNR=30 dB in the blurred image. The blur size was assumed to be constant, 13 for rotation and zoom, 1 for Gaussian blur. Presented are the results of measurement on the sat\_256 image for zoom blur and on the softdots image for rotational and Gaussian blur.

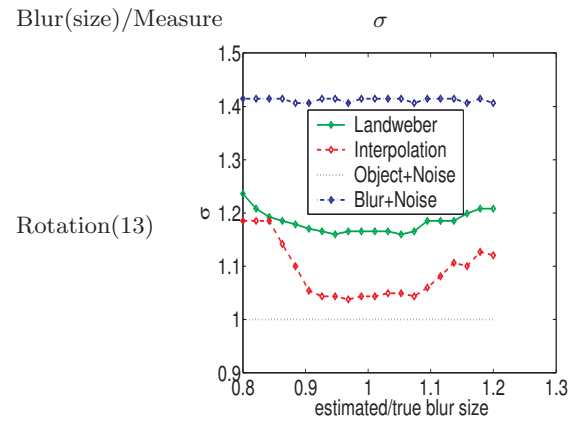


**Figure 5.14.** Change in variance of the Gaussians in the test-image as a function the accuracy of the PSF-estimate.

## 5.5 Varying number of PSF estimates

To see how the number of available PSFs affect the method blur size and noise was held constant while the number of estimated PSFs varied. The blur size was held constant at 13 for rotational and radial while the Gaussian blur size was 1. The noise level was constant at 30dB. Finally the number of estimates ranged from  $2^2$  to  $64^2$ .

The test results are shown in figure 5.5. In the figures are the SNR and ME measures for the restored images as well as for the images with only blur and noise applied.

As the number of known PSFs increases SNR increases and ME decreases. However, for the natural image this is not entirely true. When the number of PSFs reaches  $16^2$  the measurements peak and after that the results gets worse, this is explained by the edge-effects that occur due to the padding during filtering. The softdot image have solid black edges and during restoration this does not give rise to any edge-effects. What can be noted though is that the results are not getting much better past  $16^2$  even for the softdot image.

The Landweber method appears to be sensitive to the number of filter used when dealing with natural images. Above  $16^2$  filters SNR decreases substantially and ME shows the same trend. The most plausible explanation is the sectioning of the image. The Landweber method shows visual signs of segmentation and when the number of filters used increase the distortion dominates the image. In the softdots image this is not the case since most of the image is solid black. The distortion from segmentation is less obvious which also shows in the SNR and ME which both indicates that more filters is always better.

The  $\sigma$  measure, see figure 5.16, indicates that the gain in quality increases when the number of filters is increased.  $\sigma$  for both methods lies between the original image and the blurred image but interpolation methods is performing better. The image used during the  $\sigma$  measure is even more forgiving in respect to segmentation than the softdots image.

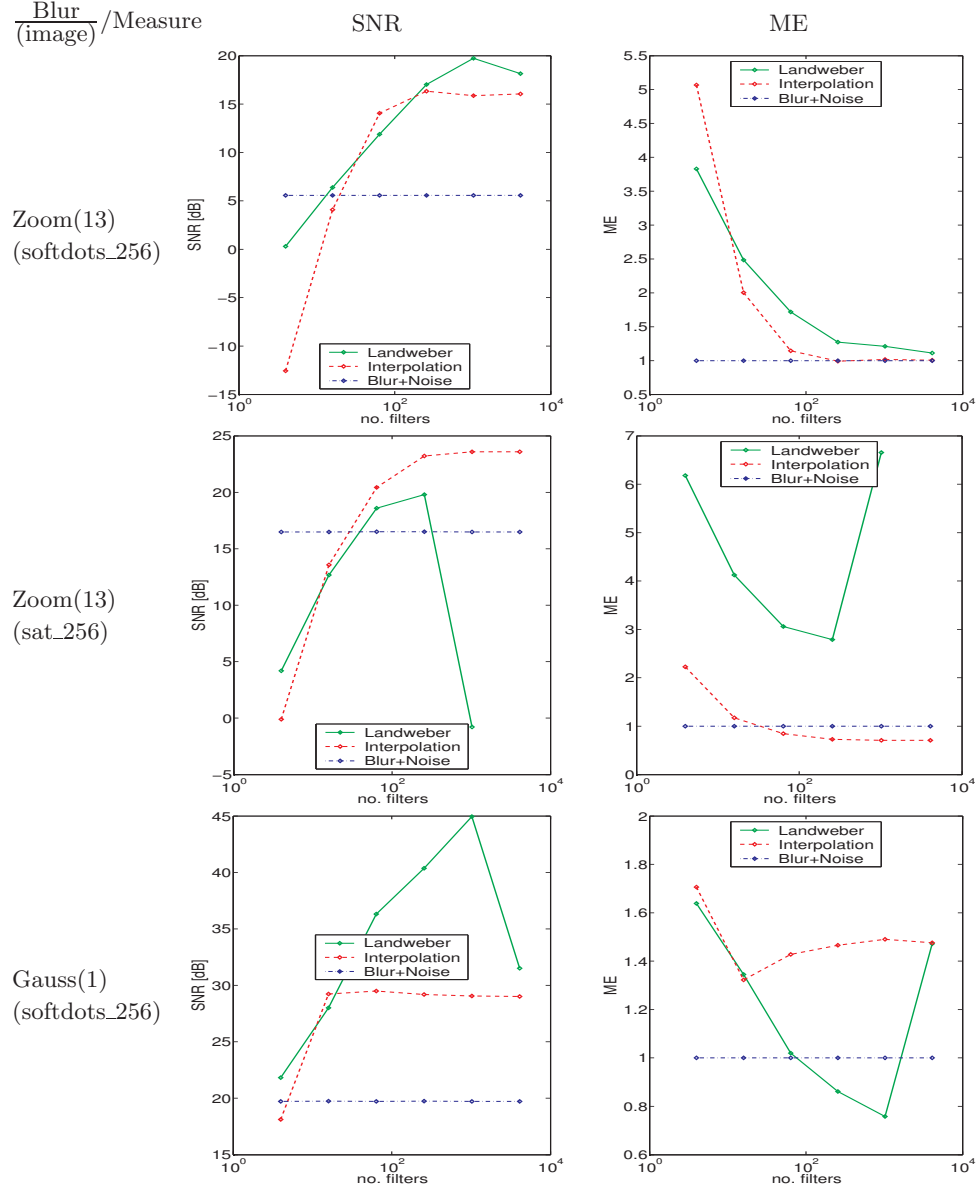


**Figure 5.15.** SNR and ME per pixel as a function of the number of estimated PSFs in restoration of the blurred images. The noise level was held constant, SNR=30 dB in the blurred image. The blur size was also constant. 13 for rotation and zoom, 1 for Gaussian blur. Presented are the results of measurement on the sat\_256 image for rotational blur and the softdots image for zoom and Gaussian blur.

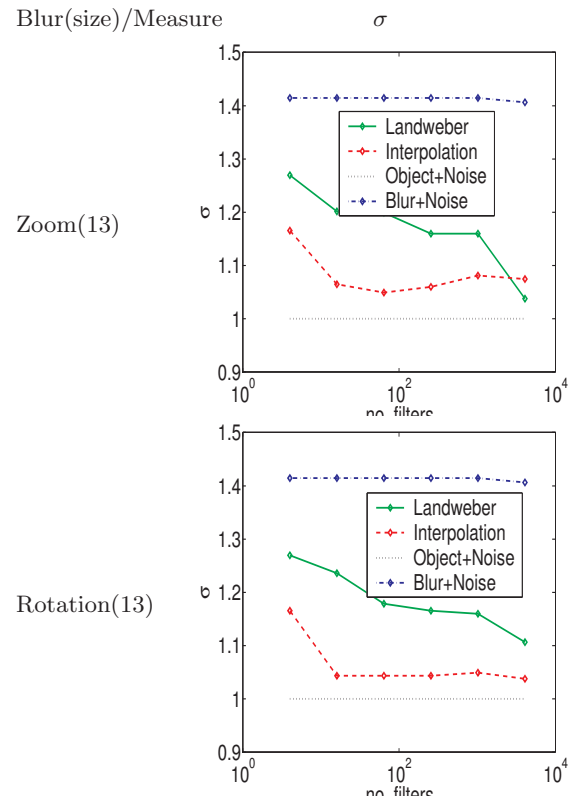


**Figure 5.16.** Change in variance of the Gaussians in the test-image as a function the number of PSF used.

## 5.6 Coma

Since coma is one of the most difficult blurs to compensate most restoration methods cannot handle it therefore the results were to be expected. The evaluation was only performed visually. The visual results are presented in figures 5.17 to 5.20 for noise level of 30 dB and figures 5.21 to 5.24 for noise level of 15 dB.

The blurred image may not look that bad and it may seem like an easy task to restore such an image. The shape of the PSF, see section 2.4, gives a notion of how difficult it may be. The way in which the true PSFs changes shape across the image makes it hard for the methods to compensate for it since it is only known in a small number of areas.

The interpolation methods relies on the fact that the PSF is slowly varying and that the unknown PSFs can be linearly interpolated, neither is true for coma in this case. This leads to the methods being unable to restore the image and even diverge after only a few iterations. Further investigation is needed since it is not adequate to interpolate the effects of coma PSFs.

The Landweber method needs the PSF to be varying slowly enough so that it can be viewed as piecewise constant. This is not true hence the Landweber methods also has troubles restoring the image. It performs slightly better than the interpolation method in restoring sharpness to the image but also introduces a lot of artifacts, especially along the edges.

As can be seen in the images restoration was not successful although some improvement can be seen. The Landweber method provides the best results.



**Figure 5.17.** sat\_256 with noise at SNR=30 dB.



**Figure 5.18.** sat\_256 with coma and noise at SNR=30 dB.



**Figure 5.19.** Blurred image restored with interpolation method..



**Figure 5.20.** Blurred image restored with Landweber method.



**Figure 5.21.** sat\_256 with noise at SNR=15 dB.



**Figure 5.22.** sat\_256 with coma and noise at SNR=15 dB.



**Figure 5.23.** Blurred image restored with interpolation method..



**Figure 5.24.** Blurred image restored with Landweber method.



## Chapter 6

# Discussion

### 6.1 Summary of results

Two methods concerning the problem of restoring images degraded by shift-variant blur have been evaluated in this report. The methods have been evaluated with regard to the amount of blur, the amount of noise, errors in the estimated PSF and the number of PSF used during restoration. Both restoration methods appear to be useful and reasonable tolerant to noise and errors in the PSF, as shown in figures 5.11 and 5.13. The gain in sharpness and detail is significant as can be seen in figure 5.3.

As mentioned before, see section 5.1.2, certain types of shift-variant blur can be restored with direct inverse methods after a suitable coordinate transform. One problem is that when there is a combination of blurs the PSF may be shift-variant even after the coordinate transform. The two methods examined does not suffer from this problem as long as the total PSF for the system is known to better than 10%, as shown in section 5.4.

According to the results in section 5.2 both methods can restore fairly large blurs.

The gain in quality is dependent on the contents of the image and the properties of the PSF. Coma is a great example. The effect is visually not that striking but since the PSF varies over the image in a way that cannot be approximated well with linear interpolation, the restoration methods only produce a small gain in quality. This becomes obvious in figure 5.6

Both restoration methods suffer from limitations but this is natural since the problem they strive to solve is very complicated. Taking the limitations into account, both methods can be implemented and used in environments where the introduced errors and noise is acceptable. One of the limitations is the need to manually trim parameters of the methods to a certain PSF since the stopping criteria are very primitive.

Designing general stopping criteria for the methods is a very difficult task hence implementing the methods to behave adaptively is difficult. At the level at which

the methods are implemented in this report, they work best in an environment where the PSF is slowly, i.e. as compensation for optical aberrations where the PSF is not varying in time at all. In such case the PSF can be calculated to almost any degree of certainty and the external parameter to take into account is basically only the noise. The restoration method then acts as part of the optical system.

Both methods handle noise in images pretty well but the Landweber method is a bit more noise tolerant.

Weighting image quality against computational cost makes the interpolation method a natural choice.

## 6.2 Further research

Adjustments could perhaps be made to the mathematical model to incorporate noise. Since noise is a common and non-trivial problem this could result in improved image quality.

The methods could be modified to produce images optimal in different ways depending on the use of the final image. Perhaps spatially varying quality demands, concentrating the efforts of restoration in different areas of the image.

Since the restoration methods only have been tested with synthetic blur their performance on images degraded by “real” blur can only be estimated. There should not be any problems though as long as the PSF estimate is accurate enough. As shown in section 5.4 both methods tolerate small errors in the PSF estimate.

Concerning blurs such as coma further investigations are needed. The two methods in this report both produce images with slightly better sharpness but also introduces a lot of distortions. A way to correctly “interpolate” the effects of coma PSFs is needed for the interpolation method to work.

The  $\sigma$ -measure used in this report should perhaps be further investigated. Using more test images with Gaussian bells at many different radii may result in a good indication of the quality gain in different parts of the image.

## 6.3 Fulfillment of goals

As far as the postulated goals are concerned they are all fulfilled. Two methods have been investigated, implemented and thoroughly tested. The goal was not to produce an optimized algorithm for implementation in a existing system, but to investigate wether there exists a suitable method.

# Bibliography

- [1] Infrared detector arrays for thermal imaging tutorial. Web page. URL: <http://www.acreo.se>, downloaded 2005-01-25.
- [2] Mortimer Abramovitz, H. Ernst Keller, Kenneth R. Spring, Brian O. Flynn, John C. Long, Matthew J. Parry-Hill, and Michael W. Davidson. Optical aberrations. Web page. URL: <http://micro.magnet.fsu.edu/primer/anatomy/aberrationhome.html>, downloaded 2004-12-16.
- [3] R. Barrett, M. Berry, T. F. Chan, J. Demmel, J. Donato, J. Dongarra, V. Eijkhout, R. Pozo, C. Romine, and H. Van der Vorst. *Templates for the Solution of Linear Systems: Building Blocks for Iterative Methods*. SIAM, Philadelphia, PA, 1994.
- [4] Ronald N. Bracewell. *The Fourier Transform & Its Applications*. McGraw-Hill Science/Engineering/Math, 3 edition, June 1999.
- [5] Rafael C. Gonzalez and Richard E. Woods. *Digital Image Processing*. Prentice Hall, 2nd edition, January 2002.
- [6] Peter Hackman. *Boken med kossan på*. 4th edition, 1999.
- [7] E. Hecht. *Optics*. Addison Wesley, 4 edition, August 2001.
- [8] H. Hong and T. Zhang. Fast restoration approach for rotational motion blurred image based on deconvolution along the blurring paths. *Optical Engineering*, 42:347–3486, December 2003.
- [9] L. Landweber. An iteration formula for fredholm integral equations of the first kind. *Amer. J. Math*, 73:615–624, 1951.
- [10] Lei Liang and Yuanchang Xu. Adaptive landweber method to deblur images. *IEEE Signal Processing Letters*, 10(5):129–132, 2003.
- [11] Peter Ljungberg, Alf Elg, and Elisabeth Gårdbäck. Metoder för minskning av rörelseeffekter vid långa integrationstider. Technical Report LiTH-ISY-I-1338, Saab Bofors Dynamics AB, April 2004. 27.

- 
- [12] James G. Nagy and Dianne P. O’Leary. Restoring images degraded by spatially variant blur. *SIAM Journal on Scientific Computing*, 19(4):1063–1082, 1998.
  - [13] Jonathan Richard Shewchuk. An introduction to the conjugate gradient method without the agonizing pain. Internet, August 1994. Edition 1 $\frac{1}{4}$ .
  - [14] Eva Sjöström. *Singular Value Computations for Toeplitz Matrices*. Licentiate thesis LiU-TEK-LIC-1996:19, Department of Mathematics , Linköping University, Linköping, Sweden, April 1996.
  - [15] H. J. Trussel and S. Fogel. Identification and restoration of spatially variant motion blurs in sequential images. *IEEE Transactions on Image Processing*, 1(1):123–126, 1992.
  - [16] Richard H. Vollmerhausen and Ronald G. Driggers. *Analysis of Sampled Imaging Systems*, volume TT39 of *Tutorial Texts in Optical Engineering*. SPIE, P.O. Box 10 Bellingham Washington 98227-0010, 1st edition, 2000.

## Appendix A

# Fast matrix-vector multiplication

Computing a matrix-vector multiplication for a large matrix is very costly. For a dense  $m \times n$  matrix the cost is  $mn$  complex multiplications. For a circulant matrix, described below, the FFT [4] can be used to gain performance and the cost is then  $O((m+n)\log_2(m+n))$  complex multiplications. By embedding a toeplitz matrix in a circulant matrix, preferably of a size equal to a power of two, the fast algorithm can be used on toeplitz matrices as well [14].

### A.1 Circulant matrices

A circulant matrix is completely defined by its first column, which in conjunction with the Fourier transform can be utilized to perform a cost-effective matrix-vector multiplication. Calculating the multiplication between a circulant matrix  $C$  and a vector  $x$  with the fast algorithm is performed as

$$\mathbf{y} = \mathbf{C}\mathbf{x} = \mathcal{F}^{-1}(\mathcal{F}(\mathbf{x}) \cdot \mathcal{F}(\mathbf{C}_v)) \quad (\text{A.1})$$

### A.2 Toeplitz matrices

To perform the fast multiplication between a toeplitz matrix and a vector it has to be embedded in a circulant matrix. This is accomplished by utilizing that a toeplitz matrix is completely defined by its first row and first column. A  $m \times n$  toeplitz matrix is defined by

$$t_{col} = \begin{pmatrix} x_m \\ x_{m-1} \\ \cdot \\ \cdot \\ x_1 \end{pmatrix}, \quad t_{row} = \begin{pmatrix} x_{m+n-1} \\ x_{m+n-2} \\ \cdot \\ \cdot \\ x_{m+1} \end{pmatrix} \quad (\text{A.2})$$

With these vectors the first column of a circulant matrix, which defines the whole circulant matrix, can be formed as

$$c = \begin{pmatrix} t_{col} \\ 0 \\ t_{row} \end{pmatrix} \quad (\text{A.3})$$

The number of zeros placed between the column and row in  $c$  is chosen so that the length of  $c$  is a power of two. This to maximize performance of the FFT.

The evaluation of  $\mathbf{H}\mathbf{x}$ , where  $\mathbf{H}$  is toeplitz, is then performed as

$$\tilde{\mathbf{y}} = \tilde{\mathbf{C}}\tilde{\mathbf{x}} \quad (\text{A.4})$$

Where  $\mathbf{H}$  is embedded in  $\tilde{\mathbf{C}}$  as described above and  $\mathbf{x}$  is embedded in  $\tilde{\mathbf{x}}$  to match the size of  $\tilde{\mathbf{C}}$

$$\tilde{\mathbf{x}} = \begin{pmatrix} x \\ 0 \end{pmatrix} \quad (\text{A.5})$$

The resulting vector,  $\mathbf{y}$ , is then obtained by extracting the  $m$  first elements of  $\tilde{\mathbf{y}}$ .

## Upphovsrätt

Detta dokument hålls tillgängligt på Internet – eller dess framtida ersättare – under 25 år från publiceringsdatum under förutsättning att inga extraordinära omständigheter uppstår.

Tillgång till dokumentet innebär tillstånd för var och en att läsa, ladda ner, skriva ut enstaka kopior för enskilt bruk och att använda det oförändrat för icke-kommersiell forskning och för undervisning. Överföring av upphovsrätten vid en senare tidpunkt kan inte upphäva detta tillstånd. All annan användning av dokumentet kräver upphovsmannens medgivande. För att garantera äktheten, säkerheten och tillgängligheten finns lösningar av teknisk och administrativ art.

Upphovsmannens ideella rätt innefattar rätt att bli nämnd som upphovsman i den omfattning som god sed kräver vid användning av dokumentet på ovan beskrivna sätt samt skydd mot att dokumentet ändras eller presenteras i sådan form eller i sådant sammanhang som är kränkande för upphovsmannens litterära eller konstnärliga anseende eller egenart.

För ytterligare information om Linköping University Electronic Press se förlagets hemsida <http://www.ep.liu.se/>

## Copyright

The publishers will keep this document online on the Internet – or its possible replacement – for a period of 25 years starting from the date of publication barring exceptional circumstances.

The online availability of the document implies permanent permission for anyone to read, to download, or to print out single copies for his/hers own use and to use it unchanged for non-commercial research and educational purpose. Subsequent transfers of copyright cannot revoke this permission. All other uses of the document are conditional upon the consent of the copyright owner. The publisher has taken technical and administrative measures to assure authenticity, security and accessibility.

According to intellectual property law the author has the right to be mentioned when his/her work is accessed as described above and to be protected against infringement.

For additional information about the Linköping University Electronic Press and its procedures for publication and for assurance of document integrity, please refer to its www home page: <http://www.ep.liu.se/>.